iScience

Article

Endosomal protein DENND10 promotes developmental competence of neurite extension

Graphical abstract

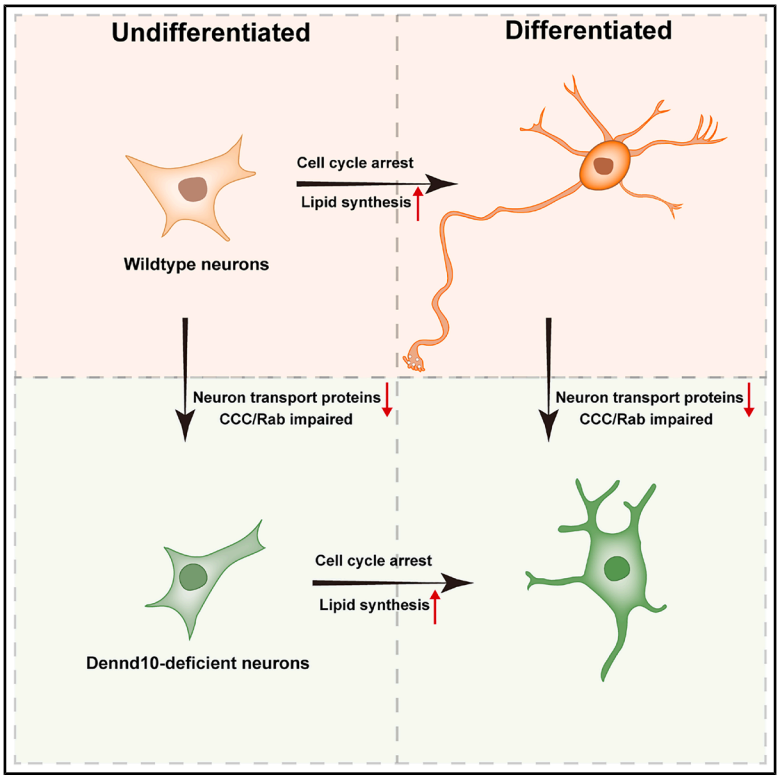

Highlights

- Endosomal protein DENND10 promotes neurite outgrowth
- Neurite outgrowth involves two distinct and largely orthogonal processes
- Rab activation and the CCC complex are downstream of DENND10 in neuritogenesis

Authors

Aiqing Li, Jie Zhang, Chao Ma, ..., Jianrui Song, Yaobo Liu, Yanling Zhang

Correspondence

jianrui.song@xjtlu.edu.cn (J.S.), liuyaobo@suda.edu.cn (Y.L.), yanlzhan@suda.edu.cn (Y.Z.)

In brief

Natural sciences; Biological sciences; Neuroscience; Molecular neuroscience; Cellular neuroscience

Li et al., 2025, iScience *28*, 112385
May 16, 2025
https://doi.org/10.1016/j.isci.2025.112385

CellPress

iScience

CellPress
OPEN ACCESS

Article

Endosomal protein DENND10 promotes developmental competence of neurite extension

Aiqing Li,[1,6] Jie Zhang,[1,6] Chao Ma,[1,6] Lijuan Qi,[1] Qiuming Hu,[1] Qian Li,[1] Yufei Fang,[3] Jianrui Song,[3,*] Yaobo Liu,[2,4,*] and Yanling Zhang[1,5,7,*]

[1]School of Life Sciences, Suzhou Medical College of Soochow University, Suzhou 215123, China
[2]Jiangsu Key Laboratory of Neuropsychiatric Diseases and Institute of Neuroscience, Clinical Research Center of Neurological Disease, The Second Affiliated Hospital of Soochow University, Soochow University, Suzhou, Jiangsu 215123, China
[3]Wisdom Lake Academy of Pharmacy, Jiangsu Provincial Higher Education Key Laboratory of Cell Therapy Nanoformulation (Construction), Suzhou Municipal Key Lab of Metabolic Syndrome and Drug Research, School of Science, Xi'an Jiaotong-Liverpool University, Suzhou 215123, China
[4]Department of Rehabilitation Medicine, The Fourth Affiliated Hospital of Soochow University, Suzhou 215123, China
[5]MOE Key Laboratory of Geriatric Diseases and Immunology, Suzhou Medical College of Soochow University, Suzhou 215123, China
[6]These authors contributed equally
[7]Lead contact
*Correspondence: jianrui.song@xjtlu.edu.cn (J.S.), liuyaobo@suda.edu.cn (Y.L.), yanlzhan@suda.edu.cn (Y.Z.)
https://doi.org/10.1016/j.isci.2025.112385

SUMMARY

A distinguishing feature of neurons is the presence of long neurites that enable far-reaching communication. Establishing this complex morphology requires precise regulation of intracellular transport and signaling. Our study identifies DENND10, an ancient endosomal protein, as a crucial factor in shaping neuron morphology. DENND10 is a potential regulator of Rab GTPase signaling and interacts with the CCC/Retriever endosomal complex. Loss of DENND10 in a neuronal cell culture model resulted in shortened neurites. Quantitative proteomics revealed two distinct processes of neurite outgrowth: differentiation-induced biochemical changes and a pre-existing vesicular transport system modulated by DENND10. Mechanistically, both Rab27 and CCC complex subunit CCDC22 act downstream of DENND10 to support neurite extension. In primary cortical neurons, loss of DENND10 or CCDC22 led to shortened dendrites and impaired axon development. These findings provide a conceptual framework for neuronal morphogenesis during differentiation and highlight the critical role of DENND10/CCC in neurite extension.

INTRODUCTION

Neurons are highly specialized cells with characteristically long neurites and intricate synaptic structures that enable long-distance direct communication between cells. These unique morphological features impose high demands on their intracellular membrane transport system. Accordingly, alterations in endosomal transport pathways in humans are often associated with neurodegenerative diseases, including Alzheimer's disease and Parkinson's disease.[1–3] Therefore, it is crucial to elucidate neuron-specific roles of membrane transport pathways.

Vesicle transport activities are closely linked to the growth of neurites.[4] The bi-directional transport of endosomes/lysosomes along microtubule tracks within neurites is critical for the growth and maintenance of dendrites and axons.[5] During neurite outgrowth, the surface area and surface-to-volume ratio of a neuron increase dramatically, typically by ~20% per day.[6] A crucial source of membrane expansion is provided by exocytic vesicular transport pathways, such as recycling endosomes and secretory vesicles, which deliver membrane components into the plasma membrane.[7–10] A major class of regulators in vesicle trafficking is the Rab family of small GTPases. Rab proteins act as molecular switches, cycling between an active GTP-bound state and an inactive GDP-bound state.[11] Interestingly, about half of the Rab isoforms in fruit flies exhibit neuron-specific or neuron-enriched expression.[12] A number of Rabs, including Rab11, Rab35, Rab5, Rab4, Rab7, Rab33a, and Rab10, have been found to play important roles in neurite outgrowth.[13] Consistently, deficiencies in Rab proteins have been linked to various diseases, particularly neurological disorders.[14–16]

The activation of Rab proteins from GDP-bound state to GTP-bound state is catalyzed by guanine nucleotide exchange factors (GEFs). The DENN (differentially expressed in normal cells and neoplasia) domain-containing proteins represent the largest family of GEFs for Rab GTPases,[17] particularly those involved in exocytic pathways.[18] The DENN domain is evolutionarily ancient, originating in the common eukaryotic ancestor around

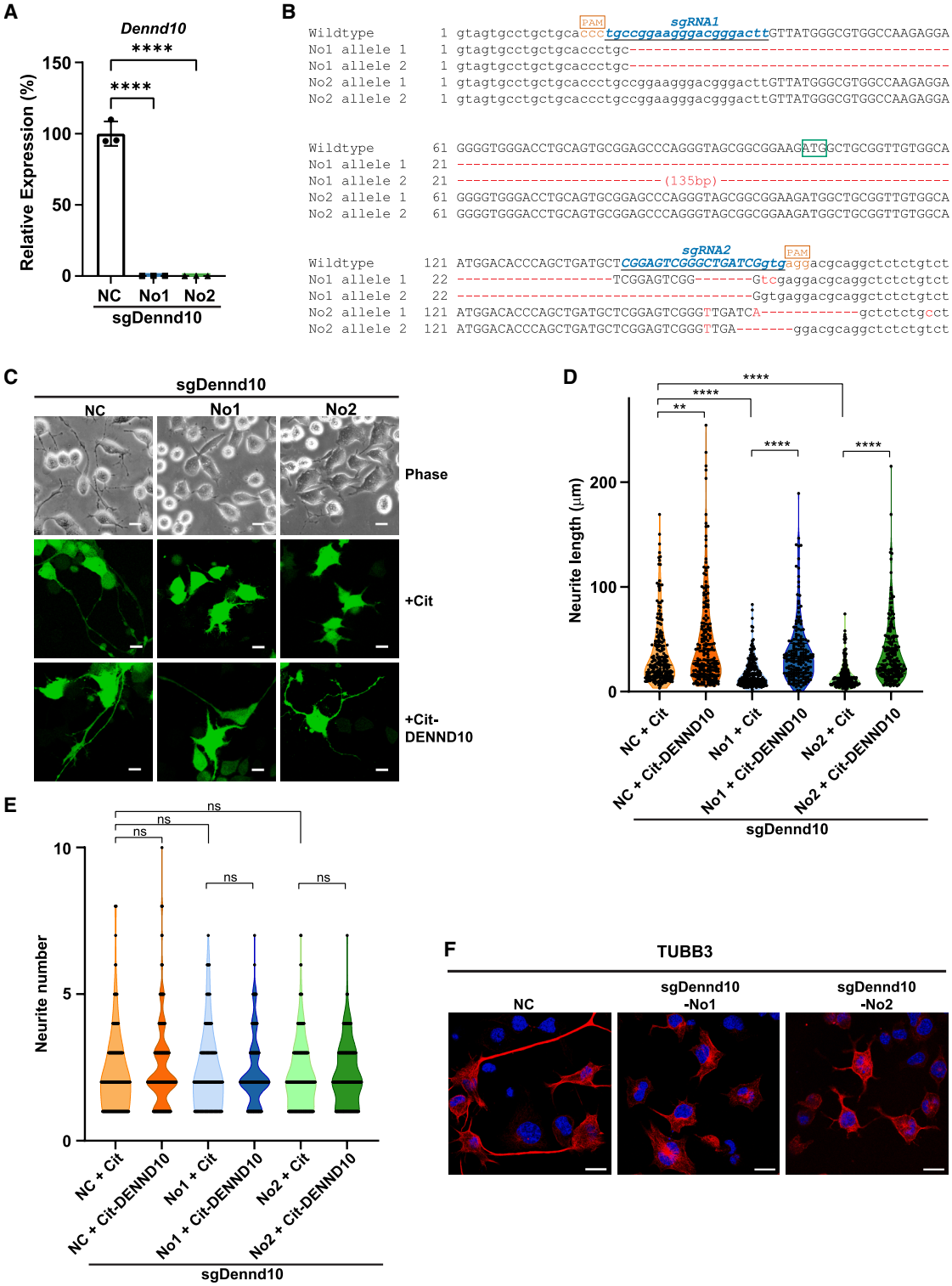

Figure 1. *Dennd10* deficiency impairs neurite outgrowth

(A) Expression of *Dennd10* mRNA in non_targeting (NC) and two clonal sgDennd10 CAD cell lines (No1 and No2) measured by qPCR. Data are presented as mean ± SD (n = 3). Significance was determined by one-way ANOVA followed by post hoc multiple-comparison test. ****, $p < 0.0001$.

(B) Sanger sequencing of the *Dennd10* genomic region in the sgDennd10 cell lines. The two targeting sgRNA and their PAM sequences are highlighted in blue and orange, respectively. The start codon within Exon1 is indicated with a green box.

(legend continued on next page)

two billion years ago.[19] Mutations in DENN-domain containing proteins have been linked to several neurological and neurodevelopmental disorders, including intellectual disability associated with DENND2B/ST5[20] and DENN/MADD,[21] Charcot-Marie-Tooth neuropathy type 4B attributed to SBF1 and SBF2,[22] and the occurrence of amyotrophic lateral sclerosis and frontotemporal dementia associated with DENND9/C9ORF72.[23]

DENND10 (formerly known as FAM45A) is a unique member of the DENN-domain containing protein family. While it shares higher-order structural similarity with classical DENN domain proteins, its primary sequence diverges significantly.[24] In a previous study, we found that DENND10 is mainly localized in endosomes and lysosomes, where it regulates the positioning, maturation, and secretion of endosomes.[24] However, the physiological roles of DENND10, particularly in the nervous system, remain little understood.

Interestingly, DENND10 has recently been identified as an integral subunit of the CCC/Retriever complex on endosomes in several structural studies.[25–27] Many large multi-protein complexes, including Retromer (VPS26, VPS35, VPS29), Retriever (VPS26C, VPS35L, VPS29), CCC (CCDC22, CCDC93, COMMD), and WASH (WASP and scar homology) complexes, are known to regulate the exocytic traffic from endosomes.[28–30] These complexes work coordinately to recycle membrane components back to the plasma membrane via tubulo-vesicular carriers. CCC and Retriever are often co-purified together and sometimes collectively referred to as the Commander complex.[31] While the precise role of DENND10 within the CCC/Retriever complex remains unclear, its depletion has been shown to impair the sorting of Retromer cargoes.[32] Notably, these exocytic complexes are closely related to human neuropathies. Mutations in Retromer subunits cause late-onset Parkinson's disease[33–35] or atypical parkinsonism,[36] while mutations in Retriever, CCC, and WASH complexes have been linked to intellectual disability and 3C/Ritscher-Schinzel syndrome.[37–41] Reduced expression of Retromer-related proteins has also been frequently observed in Alzheimer's disease.[42] These disease associations highlight the critical role of endosomal sorting complexes in the nervous system.

In this study, we demonstrated that DENND10 plays a crucial role in neurite extension using CRISPR gene editing. Quantitative proteomics revealed two distinct molecular processes during neuronal differentiation. The first involves differentiation-induced biochemical alterations, such as cell cycle exit and up-regulation of lipid biosynthesis enzymes. The second process highlights a pre-existing vesicular transport system modulated by DENND10. DENND10 deficiency did not affect the differentiation process *per se,* but suppressed the expression of multiple neuron-specific genes prior to differentiation. Mechanistically, DENND10 exerts its influence by regulating both Rab GTPases and the CCC/Retriever complex. These findings underscore the importance of DENND10 in the nervous system and provide a framework for the interplay between endosomal transport and neuronal morphogenesis.

RESULTS

DENND10 is involved in neurite extension

To this end, DENND10 had no known physiological functions yet. Given associations between endosomal transport and neuronal diseases, we decided to examine neuronal roles of DENND10 using mouse CAD cells as a model. CAD cells are an excitable catecholaminergic neuronal cell line derived from the central nervous system.[43,44] Upon serum withdrawal, these cells undergo differentiation and extend long neurites packed with parallel microtubules and intermediate filaments.[43] Their neurite terminals are abundant in vesicles,[43] resembling the growth cones of primary neurons.[6] CAD cells have been widely used in the literature to investigate neuronal differentiation,[45] neurite outgrowth,[46] transport within neurites,[47,48] and neuronal degeneration.[49] Therefore, they offer a valuable model for studying the role of DENND10 in neurite growth during neuronal differentiation.

To downregulate the expression of *Dennd10*, we employed lentivirus-mediated CRISPR/Cas9 gene editing in CAD cells. Since *Dennd10* has multiple splicing isoforms, a dual-guide RNA strategy was used to target Exon_1, which is present in all splicing isoforms and contains the start codon. Two independent clonal lines, designated sgDennd10_No1 and sgDennd10_No2, were established, both exhibiting nearly undetectable *Dennd10* mRNA expression (Figure 1A). The edited genomic region was confirmed by Sanger sequencing (Figure 1B). In sgDennd10_No1, a large deletion encompassing most of Exon_1 was observed, whereas sgDennd10_No2 showed disruption of the 5′ splicing donor site of the subsequent intron (Figure 1B). It should be added that low levels of peptides from the C-terminal DENND10 sequence were detected in sgDennd10_No2 by mass spectrometry (see below, Table S1), likely due to truncated protein expression from cryptic alternative splicing events, a phenomenon observed in approximately 50% of CRISPR-edited cells.[50] Thus, these two clones represented *Dennd10* knockout or hypomorphic cells and were used in subsequent experiments.

Interestingly, neurites of differentiated CAD cells infected with the non-targeting control vector (NC) were long and thick, whereas those of the sgDennd10 cells were significantly shorter and thinner (Figure 1C). On average, neurite lengths in differentiated sgDennd10_No1 and No2 cells were approximately 34% and 24% of those in NC cells, respectively (Figures 1C and 1D). A similar reduction in neurite length was observed with

(C) Representative images of NC and sgDennd10 CAD cells after differentiation. Top: phase-contrast microscope. Middle and bottom: Cells were transfected with Citrine (Cit) or Cit-DENND10 plasmids and imaged using a fluorescence microscope. Scale bar: 15 μm
(D) Quantification of neurite length in (C). The longest neurite was measured for each cell. From left to right: n = 208, 218, 207, 189, 220, and 192 cells, respectively, from six independent experiments.
(E) Quantification of neurite number per cell in (C). From left to right: n = 191, 200, 162, 170, 204, and 189 cells, respectively, from six independent experiments. Significance in (D) and (E) was determined by one-way ANOVA followed by post hoc multiple-comparison tests. **, $p < 0.01$; ****, $p < 0.0001$; ns, non-significant.
(F) TUBB3 staining in NC and sgDennd10 by immunofluorescence. Scale bars, 15 μm.

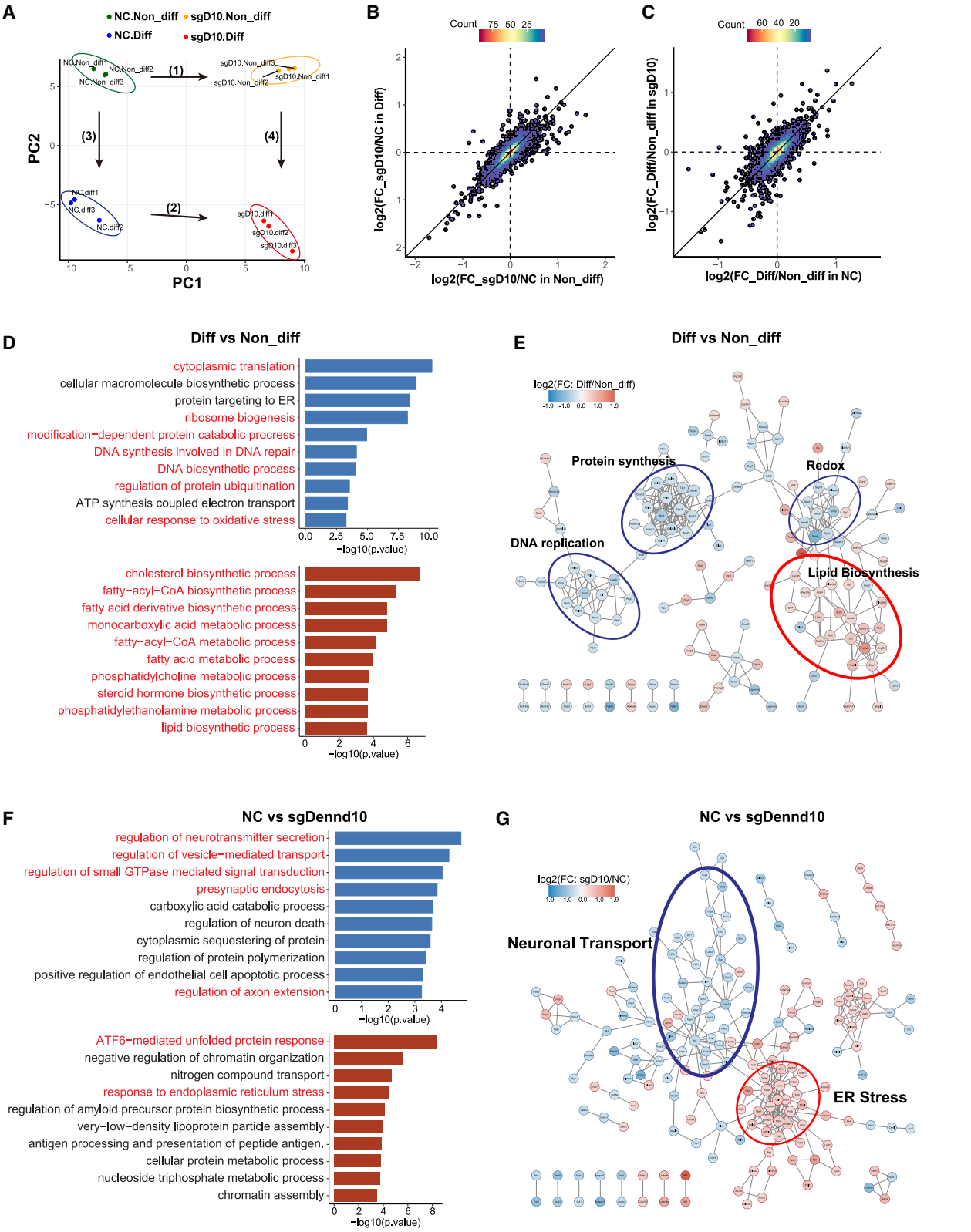

(legend on next page)

two independent plasmid-based short hairpin RNA (shRNA) constructs targeting *Dennd10* (Figures S1A–S1C). The number of neurites did not significantly change in either sgDennd10 (Figure 1E) or *Dennd10*-shRNA cells (Figure S1D), suggesting that DENND10 was not essential for the initiation of neuritogenesis. Consistent with the neurite shortening phenotype in *Dennd10*-deficient neurons, TUBB3, a neuron-specific cytoskeletal protein required for neurite extension,[51] was predominantly localized to the neurites in NC cells but was mainly confined to the soma in sgDennd10 cells (Figure 1F). Importantly, re-introducing exogenous Citrine-DENND10 protein rescued the neurite shortening defect in sgDennd10 cells (Figures 1C and 1D). Compared to cells expressing Citrine alone, sgDennd10 cells with Citrine-DENND10 expression exhibited significantly longer neurites ($p < 0.0001$), comparable to those in NC cells, confirming that the neurite shortening defect was indeed caused by the loss of DENND10 function. Notably, overexpression of DENND10 proteins also increased neurite lengths by ~20% in NC cells (Figure 1D), consistently with a positive regulatory role of DENND10 in neurite extension. Together, these results indicate that DENND10 is required for proper neurite outgrowth.

Changes in proteomic landscape during neurite outgrowth

To systematically investigate the effects of *Dennd10* deficiency on neurite outgrowth, we conducted Tandem Mass Tag (TMT)-based quantitative mass spectrometry on NC and sgDennd10_No2 cells, both in non-differentiated (denoted as NC.Non_diff and sgD10.Non_diff) and differentiated (denoted as NC.diff and sgD10.diff) states. Three biological replicates were used for each condition, totaling 12 samples. Each sample was labeled with a unique TMT-16plex mass tag, which allows parallel multiplexing and accurate comparison across samples.[52] In total, 6997 proteins were identified, of which 6910 proteins were quantifiable (Table S1). Principal component analysis (PCA) was used to visualize the overall data structure (Figure 2A). The first principal component (PC1) displayed a strong correlation with the genotypes (NC vs. sgDennd10), while the second principal component (PC2) was associated with the differentiation condition (Non-diff vs. diff), separating the samples into four distinct clusters. Intriguingly, these clusters formed a rectangle-like shape on the PCA plot. The edges representing *Dennd10* deficiency-related changes (Edge 1 and 2 in Figure 2A) were nearly orthogonal to those representing differentiation-related changes (Edge 3 and 4 in Figure 2A), suggesting that two distinct processes were involved in neurite outgrowth. Fold changes (FCs) for all quantifiable proteins were calculated along each edge. Consistently with the PCA plot, FCs along Edges 1 and 2 closely aligned with the diagonal line ($y = x$) (Figure 2B), suggesting similar effects of *Dennd10* deficiency in both non-differentiated and differentiated cells. A comparable pattern was observed for FCs along Edges 3 and 4 (Figure 2C), indicating that differentiation induced consistent changes in both sgDennd10 and NC cells.

Given the experimental design, we employed a two-way ANOVA model (~ Genotype + Differentiation + Genotype: Differentiation) to simultaneously assess the effects of *Dennd10* deficiency (Genotype), neuronal differentiation (Differentiation), and their potential interactions. Differentially expressed proteins (DEPs) were determined between the two genotypes (NC vs. sgDennd10) and across differentiation states (Non-diff vs. diff). After adjustment for multiple comparisons, we identified 4046 proteins that were significantly up- or downregulated (FDR <0.05) for the Genotype factor, 3683 proteins significantly altered for the Differentiation factor, and 139 proteins that exhibited significant interaction effects between Genotype and Differentiation (Table S1). We further focused on DEPs with FC greater than 1.3, which resulted in 363 DEPs for Genotype and 181 DEPs for Differentiation (Table S2). Volcano plots and heatmaps illustrating these DEPs are displayed in Figure S2.

To gain insights into the biological changes during neuronal differentiation, the list of DEPs for Differentiation was examined for enrichment of gene ontology terms (Figures 2D; Table S3). Additionally, we also employed the STRING database[53] to visualize protein-protein interaction network within the list (Figure 2E). It is well-known that neuronal differentiation is accompanied by cell cycle exit.[54] Consistent with this, we observed a significant down-regulation of proteins involved in DNA biosynthesis and repair (POLD1, POLD3, POLE, and POLE2) (Figures 2D and 2E). Also downregulated were proteins involved in protein ubiquitination and neddylation (NDFIP1, UBE2C, SQSTM1, RNF149, etc.), cytoplasmic translation (RPS25, RPS16, RPL34, RPLP1, etc.), and redox responses (GPX1, TXNRD1, HMOX1, SELENOS, etc). Conversely, DEPs that were up-regulated after differentiation

Figure 2. Proteomics landscape of NC and sgDennd10 cells before and after differentiation

(A) PCA plot displaying a low-dimensional projection of all twelve samples. The four biological groups, non-differentiated NC (NC.Non_diff), non-differentiated sgDennd10 (sgD10.Non_diff), differentiated NC (NC.Diff), and differentiated sgDennd10 (sgD10.Diff), are well-separated, forming a near-rectangular pattern.

(B and C) Scattering plots illustrating log-transformed protein expression fold changes (FCs) between groups. The plot in (B) compares FCs between sgDennd10 and NC cells before and after differentiation (corresponding to Edge 1 and 2 in A). The plot in (C) compares FCs between differentiated and non-differentiated states in NC and sgDennd10 cells (corresponding to Edge 3 and 4 in A). Each dot represents one protein. A 2D histogram is overlaid on top to visualize protein density in crowded regions.

(D) Gene Ontology (GO) enrichment analysis for biological processes downregulated (top, blue) or upregulated (bottom, red) in differentiated vs. non-differentiated cells. Key pathways of special interests are highlighted in red.

(E) Protein-protein interaction network for differentially expressed proteins (DEPs) between differentiated vs. non-differentiated cells. Each node represents a protein, colored according to the log-transformed fold change between these states. Edges represent interactions or associations between proteins, based on data from the Stringdb database.

(F) GO enrichment analysis for biological processes downregulated (top, blue) or upregulated (bottom, red) in sgDennd10 vs. NC cells. Key pathways of special interests are highlighted in red.

(G) Protein-protein interaction network for DEPs between sgDennd10 and NC cells, with node colors representing log-transformed fold changes between these groups.

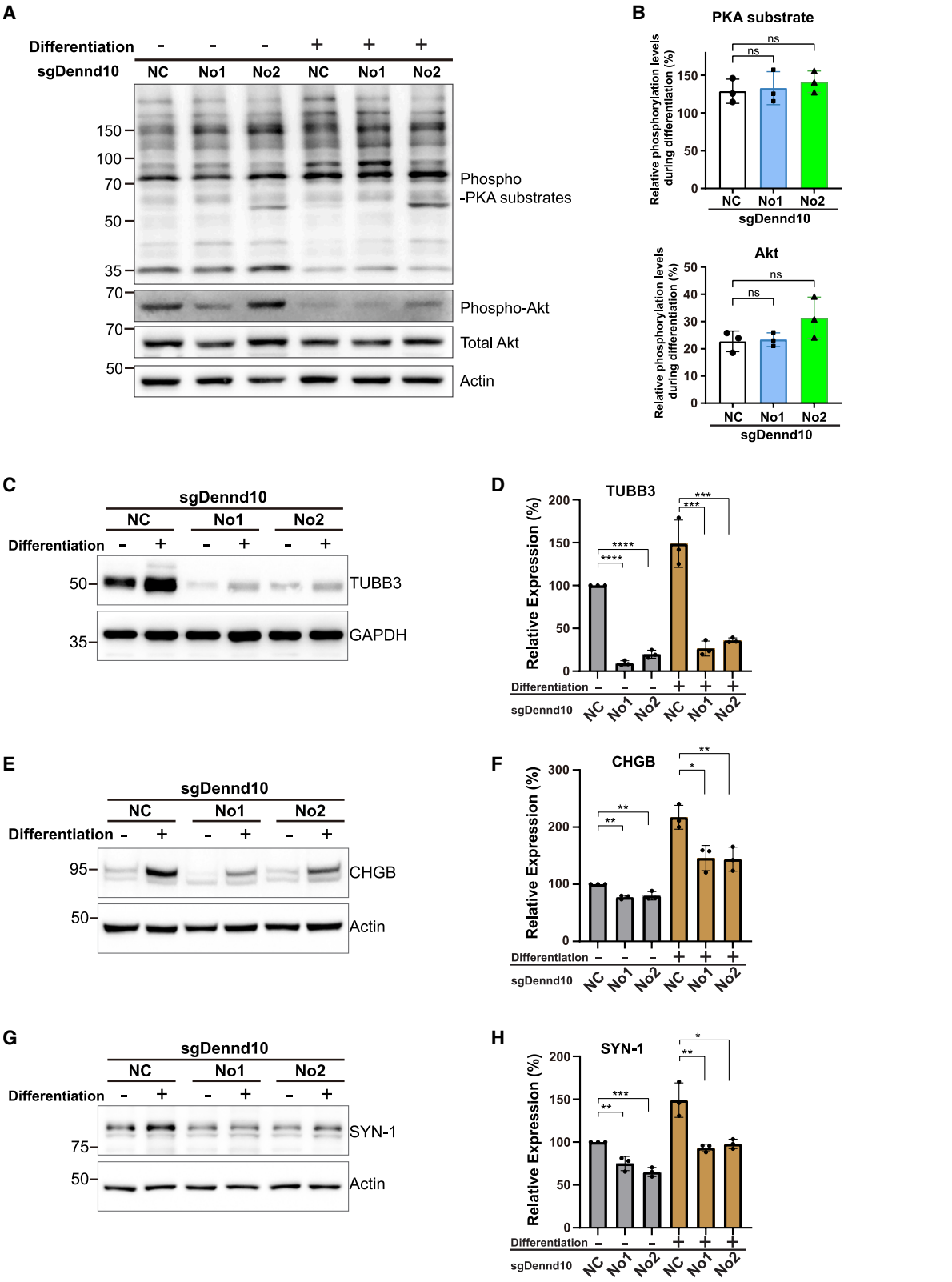

(legend on next page)

were primarily related to lipid metabolism, including enzymes for the biosynthesis of phospholipid (LPCAT3, LPIN1, and PNPLA8), sterol lipids (NSDHL, MSMO1, DHCR7, LSS, and TM7SF2) and long chain fatty acid (TECR, ACSL4, HSD17B8, and AACS) (Figures 2D and 2E). These findings are consistent with the high demand for membrane lipids during neurite outgrowth.[6] Therefore, our proteomic data effectively captured key biological processes during neuronal differentiation. Importantly, these biochemical changes occurred largely independently of DENND10, displaying similar patterns in both NC and sgDennd10 cells (Figure 2C), indicating that they are essential for neuronal differentiation but not directly related to the neurite shortening phenotype observed in sgDennd10 cells.

Similarly, we analyzed gene ontology terms (Figures 2F; Table S3) and protein interaction modules (Figure 2G) for the list of DEPs related to the Genotype factor. In sgDennd10 cells, many pathways potentially related to neuronal transport were significantly down-regulated (Figures 2F and 2G). These included proteins associated with synaptic vesicle exocytosis and recycling (SYN1, CHGB, STX1B, RIMS4, CPLX2, AMPH, PACSIN1, SNCG, SNCB, etc.), small GTPase signaling (SRC, RHOC, ARHGAP22, PLEKHG5, CHN1, etc.), and cytoskeleton organization during neurite extension (DBN1, MAPT, TPPP3, OLFM1, and TRIM46). These findings aligned with the well-established role of exocytosis and cytoskeletal dynamics in driving neurite outgrowth.[55] It has been known that microtubule-based vesicle transport is a major source of membrane expansion during neurite outgrowth.[6,7] Conversely, several molecular modules were upregulated in sgDennd10 cells, including ER-stress response proteins (ATF6B, DDIT3, CALR, ERO1A, P4HB, PDIA4, HSPA5, and HSP90B1), amino acid transporters (SLC7A5, SLC7A6, SLC3A2, SLC7A1, and SLC19A2), and histones (H2AX, H1-1, H1-2, etc.) (Figures 2F and 2G). Elevation in ER stress has also been observed in mouse brains with defective WASH complex, another endosomal sorting complex frequently associated with CCC and Retriever,[56] indicating a disruption in protein homeostasis. ER stress also plays important roles in many neurodegenerative diseases such as Alzheimer's disease[57] and Parkinson's disease.[58] Importantly, these *Dennd10* deficiency-related alterations were present in both non-differentiated and differentiated CAD cells, underscoring the role of DENND10 in modulating a network of vesicular transport pathways poised for proper neuronal morphogenesis even before differentiation.

Lastly, our two-way ANOVA model also identified some proteins that were statistically significant for the interaction term "Genotype: Differentiation" (Figure S3A; Table S3). These are proteins that exhibited distinct responses during differentiation in NC and sgDennd10 cells (i.e., off-diagonal in Figures 2B and 2C), contributing to the slight deviation from a perfect rectangular pattern in the PCA plot (Figure 2A). Gene ontology analysis revealed that this group of proteins was enriched for terms related to neuronal projection development (STMN2, STMN3, NPY, LRP12) (Figure S3B and S3C; Table S4), which is consistent with the observed differences in neurite length between NC and sgDennd10 cells.

Taken together, our proteomics dataset suggests that two distinct and largely orthogonal processes are involved in neurite extension. This two-process model resonates with earlier research which showed that *de novo* phospholipid synthesis in sprouting neurons occurs mainly in the soma (cell body), followed by an active export of newly synthesized membrane components into neurite tips, where membrane insertion typically takes place.[6,59] In this context, the two processes for neurite outgrowth revealed in our data could be interpreted as a proximal "soma" component (lipid synthesis and cell cycle exit) and a distal "neurite" component (neuronal transport and cytoskeleton track).

DENND10 regulates developmental competence for neurite outgrowth

Next, we validated our proteomic findings in both sgDennd10 lines with independent low-throughput methodology. The near orthogonal pattern observed in the PCA plot (Figure 2A) indicates that sgDennd10 experienced changes in protein level profiles similar to those of NC cells during differentiation (comparing Edge 3 and Edge 4, also see Figure 2C). To further validate this observation, we examined signaling pathways involved in differentiation in both sgDennd10 and NC cells. Differentiation of CAD cells was initiated by serum starvation, a process predicted to activate PKA signaling while attenuating Akt signaling pathways. PKA is a well-known critical regulator for neuronal differentiation,[60] while AKT is a master regulator of cell survival, growth, and proliferation.[61] We assessed PKA activities using an antibody that recognizes phosphorylated PKA substrate motif (RRXS*/T*).[62] As expected, the phosphorylation of most PKA substrates was increased in differentiated NC cells (Figures 3A and 3B). In contrast, phosphorylation of Akt decreased in NC cells, reflecting the absence of growth factors during serum withdrawal (Figures 3A and 3B). Consistent with the proteomics results, similar changes in the phosphorylation patterns of PKA substrates and Akt in sgDennd10 cells were observed (Figure 3B). This suggests that differentiation signals remained largely intact in sgDennd10 cells, indicating that the neurite shortening

Figure 3. *Dennd10* deficiency impairs neurite growth competence

(A) PKA and Akt signaling responses remained unaffected in sgDennd10 cells compared to NC cells during differentiation. Western blot analysis of phosphorylation levels of PKA substrates and Akt (Ser473), along with total Akt and actin protein levels, was performed in NC and sgDennd10 cells before and after differentiation.

(B) Quantification of phosphorylation levels of PKA substrates and Akt during differentiation in (A), expressed as percentages relative to corresponding pre-differentiation levels. The intensity of phosphorylated Akt was normalized to total Akt levels. For phosphorylated PKA substrates, the band at ~75kD, representing the highest intensity, was used as a proxy for the overall phosphorylation pattern and normalized to actin. Data are presented as mean ± SD ($n = 3$). Significance was determined by one-way ANOVA followed by post hoc multiple-comparison tests. ns, non-significant.

(C–H) *Dennd10* deficiency reduced levels of multiple neuron-related proteins before and after differentiation. Protein levels of TUBB3 (C and D), CHGB (E and F), and SYN-1 (G and H) were measured by Western blotting and quantified. Quantitation of protein levels was first normalized to GAPDH or actin and expressed as a percentage of undifferentiated NC cells. Data are presented as mean ± SD ($n = 3$). Significance was determined by one-way ANOVA followed by post hoc multiple-comparison tests. *, $p < 0.05$; **, $p < 0.01$; ***, $p < 0.001$; ****, $p < 0.0001$.

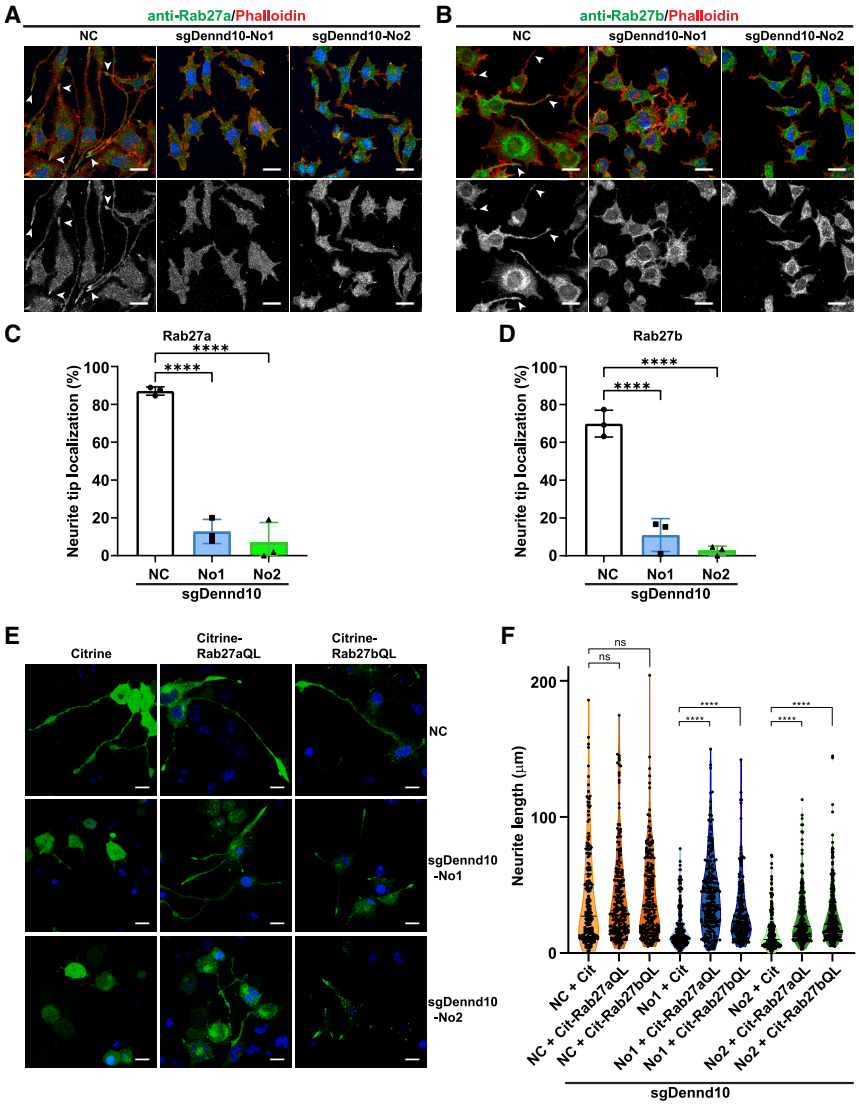

Figure 4. Rab27a and Rab27b mediate the effect of *Dennd10* deficiency on neurite length in CAD cells

(A and B) Immunofluorescence images showing the localization of endogenous Rab27a and Rab27b (green) in differentiated NC and sgDennd10 cells. Cell outlines were stained with TRITC-Phalloidin (red). Scale bars, 25 μm. Notably, neurite tip localization of Rab27 (arrowheads) was observed in both long and short neurites in NC cells.

(C and D) Quantification of Rab27a and Rab27b localization at neurite tips in (A and B). The percentage of cells displaying Rab27a/Rab27 b at neurite tips was calculated from three independent experiments. Data are presented as mean ± SD (n = 3). Significance was determined by one-way ANOVA followed by post hoc multiple-comparison tests. ****, $p < 0.0001$.

(E) Cit-Rab27aQL and Cit-Rab27bQL mutants were transfected into NC and sgDennd10 cells, followed by differentiation for 48 h. The Rab27 GTP-locked mutants rescued the neurite shortening caused by *Dennd10* deficiency. Scale bars, 15 μm

(F) Quantification of neurite lengths in (E). From left to right: n = 205, 220, 228, 223, 220, 199, 236, 226, and 240 cells, respectively, from six independent experiments. Significance was determined by one-way ANOVA followed by post hoc multiple-comparison tests. ns, non-significant; ****, $p < 0.0001$.

associated with *Dennd10* deficiency was not due to a disruption of these signaling pathways during differentiation.

Another important implication from the PCA plot (Figure 2A) is that *Dennd10* deficiency leads to similar changes in both non-differentiated and differentiated cells (comparing Edge 1 and Edge 2, also see Figure 2B). To confirm this observation, we selected three representative neuron-specific proteins, TUBB3, CHGB, and SYN1 (Synapsin-1), from the mass spectrometry results (Table S1) and examined their expression in CAD cells. TUBB3 is a cytoskeleton component implicated in neurite extension and regeneration,[51] CHGB serves as a master regulator of secretion in neurosecretory tissues,[63] and SYN-1 is an abundant synaptic vesicle-associated protein.[64] Consistent with our proteomic data, Western blotting revealed that these proteins were significantly reduced in sgDennd10 CAD cells, regardless of their differentiation status (Figures 3C–3H). A similar trend was also observed for tyrosine hydroxylase (TH), the key enzyme in the biosynthesis of the neurotransmitter dopamine (Figures S4A and S4B). Together, these results strongly suggest that DENND10 plays an important role in maintaining a pre-existing vesicular transport system that is critical for developmental competence of neurite extension prior to neuronal differentiation.

Rab27 activation is impaired in *Dennd10*-deficient neurons

We next investigated molecular mechanisms through which DENND10 influences neurite growth. Our previous study showed that DENND10 interacts with Rab27a and Rab27b in a nucleotide-dependent manner.[24] Rab27 is known to be critical for anterograde transport within neurites and synaptic vesicle exocytosis.[65,66] These functions overlap significantly with the downregulated pathways observed in sgDennd10 cells (Figure 2F), leading us to investigate the relevance of Rab27 in mediating DENND10's role in neurite outgrowth in CAD cells. First, we examined whether the activation state of Rab27 affects its subcellular localization. Citrine-tagged nucleotide-locked Rab27 mutants were introduced into CAD cells. Strikingly, The GDP-locked Rab27a-TN and Rab27b-TN mutants exhibited uniform diffusion throughout the cytoplasm, whereas the GTP-locked Rab27a-QL and Rab27b-QL mutants were enriched at the tip of neurites (Figure S5A), suggesting that active Rab27 accumulates at neurite tips, the main sites of membrane addition in developing neurons.[6] Subsequently, we assessed the localization of endogenous wild-type Rab27a and Rab27b in both NC and sgDennd10 cells using immunofluorescence

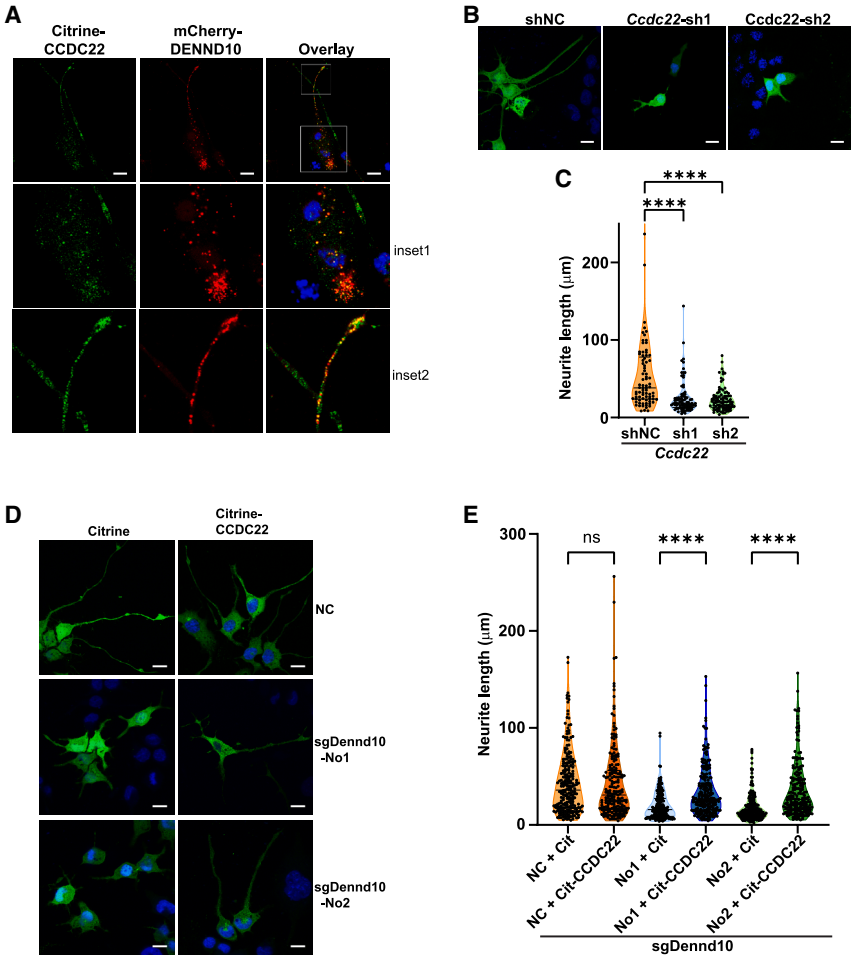

Figure 5. Neurite shortening in *Dennd10*-deficient cells could be rescued by CCDC22

(A) DENND10 co-localizes with CCDC22 in CAD cells. CAD cells were co-transfected with mCherry-DENND10 (red) and Citrine-CCDC22 (green), permeabilized with 1% saponin to remove cytosolic proteins, and then fixed. Two insets show magnified views of the soma and neurite tip region, respectively. Scale bars, 15 μm

(B) CAD cells were transfected with plasmids expressing shRNAs targeting mouse *Ccdc22* (Ccdc22-sh1 and Ccdc22-sh2) or a non-targeting control (shNC). After 24 h, cells were differentiated for another 48 h before fixation and imaging. Scale bars, 15 μm

(C) Quantification of neurite length in (B). The longest neurite was measured for each cell. From left to right: n = 81, 86, and 94 cells, respectively, from three independent experiments.

(D) Citrine or Citrine-CCDC22 plasmids were transfected into NC and sgDennd10 cells followed by differentiation for 48h. Scale bars, 15 μm

(E) Quantitation of neurite length in (D). From left to right: n = 231, 203, 214, 226, 218, and 196 cells, respectively, from six independent experiments. Significance in (C) and (E) was determined by one-way ANOVA followed by post hoc multiple-comparisons test. ns, non-significant; ****, $p < 0.0001$.

(Figures 4A–4D). In NC cells, Rab27a and Rab27b were often concentrated at neurite tips. However, in sgDennd10 cells, their localization in neurite tips was markedly reduced (Figures 4A–4D), strongly suggesting that *Dennd10* deficiency diminishes Rab27a and Rab27b activation and impairs their transport into neurites in CAD cells.

Next, we examined whether constitutively active Rab27-QL mutants could reverse the neurite shortening observed in sgDennd10 cells. These mutants are expected to bypass the requirement for GEFs such as DENND10. Citrine-tagged Rab27a-QL or Rab27b-QL mutants were transfected into NC and sgDennd10 cells (Figures 4E and 4F). We found that the expression of either Rab27a-QL or Rab27b-QL mutant significantly extended neurite lengths in both sgDennd10 cell lines (Figure 4F). In contrast, no significant enhancement was observed in NC cells, likely due to a ceiling effect for Rab27 activation under normal conditions. Additionally, the number of neurites increased to varying degrees upon expression of Rab27-QL mutants (Figure S5B), with Rab27b-QL in sgDennd10 cells showing statistically significant increases, indicating that Rab27-GTP could enhance the initiation of neuritogenesis. Taken together, these findings suggest that Rab GTPase signaling related to neurite outgrowth is downstream of DENND10 in neurite outgrowth.

Dennd10 deficiency could be rescued by CCC complex subunit CCDC22

To further investigate the mechanism of DENND10, we performed a screen for DENND10-interacting proteins using immunoprecipitation (IP). HEK293T cells were transfected with 3x-FLAG-tagged DENND10, and IP was carried out with anti-FLAG beads. Proteins co-purifing with DENND10 were identified by mass spectrometry and adjusted to the background control IP (Figure S6A; Table S4). Notably, many of the co-purified proteins were involved in endosome recycling, including CCDC22, CCDC93, COMMD3/8/9/10 (components of the CCC complex), and Vps35L (a subunit of the Retriever complex) (Figure S6A). This result confirmed several recent studies that identified DENND10 as an integral subunit of the CCC/Retriever complex.[25–27] CCDC22 was the most abundant protein in our IP (Figure S6A; Table S4). We further validated this interaction, showing that 3x-FLAG DENND10 co-precipitated with Citrine-tagged CCDC22, but not Citrine alone (Figure S6B). Additionally, in HeLa cells, mCherry-tagged DENND10 co-localized with Citrine-tagged CCDC22 on cytoplasmic vesicles, a subset of which were positive for endosomal marker CD63 (Figure S6C). In CAD cells, co-localization between Citrine-CCDC22 and mCherry-DENND10 could be observed in the soma, neurites, and neurite tips (Figure 5A). These findings demonstrate that DENND10 associates specifically and reproducibly with the CCC/Retriever endosomal complexes.

Missense mutations in CCDC22 have been associated with intellectual disability.[37,38] Previous studies reported that CCDC22

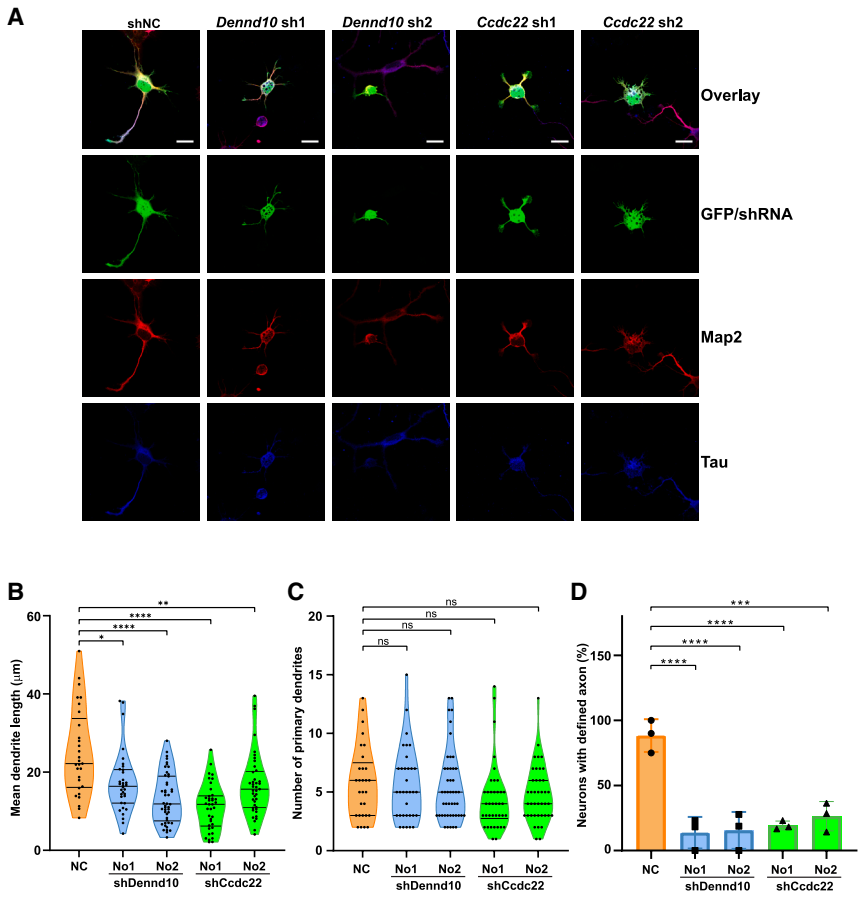

Figure 6. Loss of *Dennd10* or *Ccdc22* results in shortened dendrites and impaired axon development

(A) Primary cortical neurons were transfected with plasmids co-expressing GFP and shRNAs targeting *Dennd10* or *Ccdc22*, or a non-targeting control (shNC). Cells were replated and grown for 2 days before fixation and staining with rabbit anti-Map2 (dendrites, red) and mouse anti-Tau (axon marker, blue). Map2 and Tau were visualized using Alexa 555 donkey anti-rabbit and Alexa 647 goat anti-mouse secondary antibodies, respectively. Transfected neurons were identified by green GFP fluorescence. Scale bars, 15 μm

(B and C) Quantitation of mean dendrite length (B) and the number of primary dendrites (C) in transfected neurons. From left to right: $n = 29$, 34, 46, 38, and 41 neurons, respectively, from three independent experiments.

(D) Quantitation of the percentage of neurons with defined axons in transfected neurons. Data are presented as mean ± SD ($n = 3$ independent experiments). Significance in (B–D) was determined by one-way ANOVA followed by post hoc multiple-comparison tests. ns, non-significant; *, $p < 0.05$; **, $p < 0.01$; ***, $p < 0.001$; ****, $p < 0.0001$.

interacts with CAMSAP2, a microtubule-organizing protein involved in dendrite development,[25] suggesting a potential role for CCDC22 in neurite outgrowth. To explore this hypothesis, two independent shRNA constructs were used to knock down *Ccdc22* expression in wildtype CAD cells (Figure S7A). Both constructs significantly reduced neurite length to 47% and 43%, respectively (Figures 5B and 5C). While the number of neurites tended to decrease in *Ccdc22*-deficient cells, the change did not reach statistical significance (Figure S7B), indicating that CCDC22 is not essential for the initiation of neuritogenesis.

Given the high specificity of DENND10's association with the CCC/Retriever complex, it is reasonable to propose that DENND10 deficiency causes dysregulation within the CCC/Retriever complex, although the exact nature of this defect remains unclear. To explore the functional relationship between DENND10 and CCDC22, we employed a dosage suppression strategy[67] by overexpressing Citrine-CCDC22 or Citrine in NC and sgDennd10 cells (Figures 5D and 5E). Remarkably, Citrine-CCDC22 significantly enhanced neurite outgrowth in both sgDennd10 cell lines (Figure 5E), suggesting that the partially defective CCC/Retriever in sgDennd10 cells was compensated by the additional copies of CCDC22 proteins. While the number of neurites increased slightly after CCDC22 expression, this change did not reach statistical significance (Figure S7C). Note that CCDC22 did not significantly enhance neurite length in NC cells (Figure 5E), likely due to a ceiling effect for CCDC22 function under normal conditions.

To further investigate whether CCDC22 functions downstream of DENND10 in promoting neurite outgrowth, we overexpressed mCherry-DENND10 in wildtype CAD cells in the presence of *Ccdc22* shRNA or non-targeting control shNC (Figures S8A–S8C). In cells transfected with shNC plasmids, mCherry-DENND10 overexpression resulted in a ~19% increase in neurite length compared to mCherry control (Figure S8B), consistent with the data in Figure 1D. In contrast, when *Ccdc22* was knocked down, this effect was largely abolished, with no significant difference in neurite length observed between mCherry-DENND10 and mCherry expression (Figure S8B). Together, these findings strongly suggest that, in addition to Rab GTPases, CCDC22 also acts downstream of DENND10 to support neurite outgrowth.

DENND10 and CCDC22 are important for neurite development in primary neurons

Since neurites in CAD cells are not polarized into dendrites and axons, we next investigated the role of DENND10 and CCDC22 using primary neurons. To do this, plasmids co-expressing GFP and shRNA targeting *Dennd10* or *Ccdc22* were introduced into mouse primary cortical neurons (Figure 6A). Dendrites and axons were identified by staining with antibodies against Map2 and Tau, respectively. Consistent with our observations in CAD cells, neurons transfected with either *Dennd10* or *Ccdc22* shRNA constructs developed shorter dendrites (Figure 6B), while the number of primary dendrites remained unchanged (Figure 6C). Notably, only 14%–26% of neurons

transfected with the *Dennd10* or *Ccdc22* shRNA constructs developed a single dominant Tau+ axon after 2 days in culture, compared to ~88% of neurons transfected with the non-targeting control plasmid (shNC) (Figure 6D), suggesting impaired or delayed axon development in *Dennd10*-and *Ccdc22*-deficient neurons. These results suggest that both DENND10 and CCDC22 are critical for neurite growth and development *in vivo*.

DISCUSSION

Endosomal transport has been linked to a variety of neurological diseases.[1] In this study, we identified DENND10, an endosomal protein, as a key regulator of developmental competence of neurite extension. Our results demonstrate that DENND10 plays a crucial role in a pre-existing neuronal transport system prior to differentiation, without significantly altering the biochemical processes of differentiation such as lipid synthesis. Rab GTPase signaling and CCC complex subunit CCDC22 are downstream of DENND10 for neurite growth. These findings shed light on the molecular mechanisms through which the endosomal transport system shapes neuronal morphogenesis and could provide insights into the etiology of membrane transport-related neurological diseases.

One of the most intriguing findings from our proteomic analysis is the identification of two distinct processes driving neurite growth. On the one hand, differentiation treatment halts cell cycle and promotes lipid biosynthesis, producing surplus membrane material, as represented by Edge 3 and Edge 4 in the PCA plot (Figure 2A). On the other hand, a pre-existing membrane transport system regulated by DENND10, as represented by Edge 1 and Edge 2 in the PCA plot, is also critical for proper neurite morphogenesis. Our data showed that these two processes are largely orthogonal, suggesting that differentiation-induced biochemical changes, such as lipid biosynthesis, could be uncoupled from the DENND10-modulated transport system. First, differentiation treatment induces similar changes in *Dennd10*-deficient cells and NC cells. Protein expression FCs during differentiation remained mostly similar between NC and sgDennd10 cells (Figure 2C). Likewise, changes in the PKA and Akt signaling pathways were comparable between NC and sgDennd10 cells (Figure 3A). Second, *Dennd10* deficiency results in similar alterations in non-differentiated and differentiated CAD cells (Figure 2B). Multiple proteins involved in vesicle exocytosis and cytoskeleton organization, such as TUBB3, CHGB, and SYN-1, were decreased in both conditions (Figures 3C–3H). It can be hypothesized that DENND10-mediated membrane transport machinery helps to deliver membrane cargoes and newly synthesized lipids during neuronal differentiation, ensuring the precise deposition of these materials in the growing neurite tip. Thus, while *Dennd10* deficiency did not affect the differentiation signaling *per se*, it impaired developmental competence for neurite outgrowth even in the pre-differentiation phase.

Upregulation of a broad array of lipid biosynthesis enzymes was readily observed in differentiated CAD cells in our proteomic dataset (Figure 2D). Membrane expansion during neurite outgrowth likely necessitates the *de novo* synthesis of membrane lipids.[68] It has been shown that disruption in phospholipid synthesis leads to defective dendrite growth and maintenance in fruit flies.[69] A decrease in malonyl-CoA, the precursor of fatty acid biosynthesis, results in impaired axonal growth and reduced accumulation of late endolysosomes in axon terminals.[70] Remarkably, a human-specific allele of the TKTL1 gene, which promotes the synthesis of specific membrane lipids, has been linked to increased neocortical neurogenesis in the human lineage compared to Neanderthals.[71] Beyond providing structural support, some lipid metabolites may also serve signaling roles. For instance, a previous RNA-seq analysis on CAD differentiation identified an up-regulation of *Acss2* mRNA, which produces a nuclear pool of acetyl-CoA and promotes histone acetylation, facilitating the expression of neuron-specific genes.[45] These results highlight the importance of lipid metabolism in neuronal development. It is worth mentioning that the up-regulation of ACSS2 protein was also observed in our proteomic dataset (Table S3). Therefore, our comprehensive proteomic dataset represents a valuable resource for investigating key lipid metabolic proteins involved in neuronal morphogenesis.

DENN domains are best known for their GEF activities toward Rab proteins, which are key regulators of endosomal trafficking. Rab11 and Rab35, two small GTPases found on recycling endosomes, promote neurite outgrowth and axonal elongation.[7,13] Conversely, loss-of-function mutations or down-regulation of Rab5, Rab4, Rab35, Rab33a or Rab10 result in impaired axonal growth.[13] In this study, we demonstrated that the localization of Rab27a/Rab27 b at neurite tips was greatly diminished in *Dennd10*-deficient CAD cells, and that constitutively active Rab27-QL mutants could rescue neurite growth in sgDennd10 neurons. This indicates that Rab27 is downstream of DENND10 function in CAD cells. We noted that, in sgDennd10_No2 cells, Rab27-QL mutants did not fully restore neurite lengths to NC levels, which may be due to several reasons. First, Rab activation typically requires precise spatiotemporal regulation, which may not be fully recapitulated by constitutively active mutants. Second, other factors, such as the CCC complex and additional Rab proteins, could also function downstream of DENND10. Last but not least, sgDennd10_No2 cells contain some amount of truncated Dennd10 protein resulting from alternative splicing (Table S2), which could act in a dominant-negative manner to limit complete rescue. It is also important to recognize that the role of Rab27 in neurite growth could be context-dependent. Paradoxically, a genome-wide screening identified Rab27 and Rab3 as negative regulators of neuronal regeneration.[72] In this case, the growth cone (neurite tip) has been replaced by synaptic terminals in mature neurons[6] and Rab27 inhibition was thought to divert membrane recycling from synaptic traffic to neurite extension.

Consistent with findings from other groups,[25–27] our study demonstrated that DENND10 interacts with CCC/Retriever complex with high specificity. The role of DENND10 in this complex remains unknown. Interestingly, it was reported that DENND10/FAM45A knockout in HeLa cells did not affect the trafficking of integrin β1, a typical Retriever cargo, but instead perturbed cargo recycling of the related Retromer complex.[32] Another study indeed identified DENND10/FAM45A following the IP of the Retromer subunit.[36] Therefore, it is likely that DENND10 plays a role in the assembly and orchestration

among these multi-protein complexes such as Retromer and Retriever.

We showed that both Rab proteins and CCDC22 are downstream of the DENND10 pathway. Currently, it is not clear how the potential GEF activity of DENND10 is coordinated with its role in the CCC/Retriever complexes. Some hints may be drawn from the regulation of the Retromer complex, the most well-studied recycling coat complex. Endosomal recruitment of the Retromer requires Rab5 and Rab7.[73] TBC1D5, a GTPase-activating protein (GAP) for Rab7, is a sub-stoichiometric component of the Retromer, linking endosomal recruitment of the Retromer with the maturation of the endosomes.[29] It is conceivable that the presence of DENND10 in the CCC/Retriever could integrate cargo recycling with the positioning or maturation of the endosomes. Notably, the putative Rab binding surface of DENND10 seems to overlap with its binding surface for CCDC22/CCDC93,[25–27] suggesting potential competition or a ''handover'' mechanism. This region is inherently flexible and exhibits high conformational heterogeneity, suggesting its potential role as a regulatory site.[25] Future studies will aim to elucidate specific roles of DENND10 and its potential GEF activity within the endosomal recycling pathway.

In summary, our findings highlight the significant role of DENND10 in promoting developmental competence of neurite outgrowth by influencing Rab GTPases and the CCC complex. These findings shed light on the interplay between membrane transport and neuronal morphogenesis, offering valuable insights into the etiology of membrane transport-related neurological diseases. Importantly, these results raise important considerations regarding the timing of therapeutic interventions for neurological disorders associated with disruptions in membrane transport pathways.

Limitations of the study

The GEF activity of DENND10 for Rabs or other small GTPases remains to be fully characterized. While DENND10 interacts with Rab27 in a nucleotide-dependent manner *in vitro*,[24] we could not rule out the possibility that its influence on Rab27 activation may be indirect, potentially mediated by a signaling cascade involving other small GTPases. Furthermore, the precise mechanisms by which DENND10 functions within the CCC complex warrant additional investigation.

RESOURCE AVAILABILITY

Lead contact

Requests for further information and resources should be directed to and will be fulfilled by the lead contact, Yanling Zhang (yanlzhan@suda.edu.cn)

Materials availability

All materials and unique reagents described in this study are available from the lead contact upon reasonable request.

Data and code availability

- The mass spectrometry proteomics data in the manuscript have been deposited in the ProteomeXchange Consortium under the dataset identifier PXD038623 and are publicly available as of the date of publication.
- This paper does not report original code.
- Any additional information required to reanalyze the data reported in this paper is available from the lead contact upon request.

ACKNOWLEDGMENTS

CAD cells were a gift from the laboratory of Dr. Kristen Verhey at the University of Michigan. We thank Dr. Ying Xu at Soochow University for helping with the CRISPR plasmid design. Y.Z. is supported by the National Natural Science Foundation of China (31401220, 31571465), the Natural Science Foundation of Jiangsu Province (BK20211312), the Project of MOE Key Laboratory of Geriatric Diseases and Immunology (No. KJS2405), and a project funded by Priority Academic Programme Development of Jiangsu Higher Education Institutions (PAPD). Y.L is supported by the National Key Research and Development Program of China (2023YFC2412502, 2023YFC2306502), the National Natural Science Foundation of China (82171376, 81971164), a project funded by the Priority Academic Program Development of Jiangsu Higher Education Institutions, and the Key Research and Development Plan of Jiangsu Province (BE2023701). J.S. is supported by the Xi'an Jiaotong-Liverpool University (RDF-23-02-014). C. M. is supported by Jiangsu Funding Program for Excellent Postdoctoral Talent (2024ZB029).

AUTHOR CONTRIBUTIONS

Conceptualization, Y.Z., Y.L., J.S., A.L., J.Z., and C.M.; methodology, investigation, software, and data curation, A.L., J.Z., C.M., L.Q., Q.H., Q.L., Y.F., J.S., Y.L., and Y.Z.; writing–original draft preparation, Y.Z., A.L., J.Z., and C.M.; writing–reviewing and editing, A.L., J.Z., C.M., L.Q., Q.H., Q.L., Y.F., J.S., Y. L., and Y.Z.; supervision, J.S., Y.L., and Y.Z.; funding acquisition and resources; J.S., Y.L., and Y.Z. All authors read and approved the final manuscript.

DECLARATION OF INTERESTS

The authors declare no competing interests.

STAR★METHODS

Detailed methods are provided in the online version of this paper and include the following:

- KEY RESOURCES TABLE
- EXPERIMENTAL MODEL AND STUDY PARTICIPANT DETAILS
  - Cell culture
  - Primary cortical neurons
- METHOD DETAILS
  - Plasmids
  - Transfection in cell lines
  - Transfection in primary neurons
  - CRIPSR-mediated gene editing
  - Neurite outgrowth
  - TMT based proteomics
  - Bioinformatics data analysis of proteomics
  - Immunoprecipitation
  - Immunofluorescence
  - qRT-PCR
  - Western blotting
- QUANTIFICATION AND STATISTICAL ANALYSIS
  - Statistics

SUPPLEMENTAL INFORMATION

Supplemental information can be found online at https://doi.org/10.1016/j.isci.2025.112385.

Received: September 10, 2023
Revised: October 24, 2024
Accepted: April 4, 2025
Published: April 8, 2025

REFERENCES

1. Qureshi, Y.H., Baez, P., and Reitz, C. (2020). Endosomal Trafficking in Alzheimer's Disease, Parkinson's Disease, and Neuronal Ceroid Lipofuscinosis. Mol. Cell Biol. *40*, e00262-20. https://doi.org/10.1128/mcb.00262-20.
2. Maninger, J.K., Nowak, K., Goberdhan, S., O'Donoghue, R., and Connor-Robson, N. (2024). Cell type-specific functions of Alzheimer's disease endocytic risk genes. Philos. Trans. R. Soc. Lond. B Biol. Sci. *379*, 20220378. https://doi.org/10.1098/rstb.2022.0378.
3. Morris, H.R., Spillantini, M.G., Sue, C.M., and Williams-Gray, C.H. (2024). The pathogenesis of Parkinson's disease. Lancet (London, England) *403*, 293–304. https://doi.org/10.1016/s0140-6736(23)01478-2.
4. Humpert, I., Di Meo, D., Püschel, A.W., and Pietschmann, J.F. (2021). On the role of vesicle transport in neurite growth: Modeling and experiments. Math. Biosci. *338*, 108632. https://doi.org/10.1016/j.mbs.2021.108632.
5. Roney, J.C., Cheng, X.T., and Sheng, Z.H. (2022). Neuronal endolysosomal transport and lysosomal functionality in maintaining axonostasis. J. Cell Biol. *221*, e202111077. https://doi.org/10.1083/jcb.202111077.
6. Pfenninger, K.H. (2009). Plasma membrane expansion: a neuron's Herculean task. Nat. Rev. Neurosci. *10*, 251–261. https://doi.org/10.1038/nrn2593.
7. Quiroga, S., Bisbal, M., and Cáceres, A. (2018). Regulation of plasma membrane expansion during axon formation. Dev. Neurobiol. *78*, 170–180. https://doi.org/10.1002/dneu.22553.
8. Urbina, F.L., Gomez, S.M., and Gupton, S.L. (2018). Spatiotemporal organization of exocytosis emerges during neuronal shape change. J. Cell Biol. *217*, 1113–1128. https://doi.org/10.1083/jcb.201709064.
9. Bowen, A.B., Bourke, A.M., Hiester, B.G., Hanus, C., and Kennedy, M.J. (2017). Golgi-independent secretory trafficking through recycling endosomes in neuronal dendrites and spines. Elife *6*, e27362. https://doi.org/10.7554/eLife.27362.
10. Raiborg, C., Wenzel, E.M., Pedersen, N.M., Olsvik, H., Schink, K.O., Schultz, S.W., Vietri, M., Nisi, V., Bucci, C., Brech, A., et al. (2015). Repeated ER-endosome contacts promote endosome translocation and neurite outgrowth. Nature *520*, 234–238. https://doi.org/10.1038/nature14359.
11. Homma, Y., Hiragi, S., and Fukuda, M. (2021). Rab family of small GTPases: an updated view on their regulation and functions. FEBS J. *288*, 36–55. https://doi.org/10.1111/febs.15453.
12. Dey, G., Jaimovich, A., Collins, S.R., Seki, A., and Meyer, T. (2015). Systematic Discovery of Human Gene Function and Principles of Modular Organization through Phylogenetic Profiling. Cell Rep. *10*, 993–1006. https://doi.org/10.1016/j.celrep.2015.01.025.
13. Petrova, V., Nieuwenhuis, B., Fawcett, J.W., and Eva, R. (2021). Axonal Organelles as Molecular Platforms for Axon Growth and Regeneration after Injury. Int. J. Mol. Sci. *22*, 1798. https://doi.org/10.3390/ijms22041798.
14. Zhang, X., Huang, T.Y., Yancey, J., Luo, H., and Zhang, Y.W. (2019). Role of Rab GTPases in Alzheimer's Disease. ACS Chem. Neurosci. *10*, 828–838. https://doi.org/10.1021/acschemneuro.8b00387.
15. Bonet-Ponce, L., and Cookson, M.R. (2019). The role of Rab GTPases in the pathobiology of Parkinson' disease. Curr. Opin. Cell Biol. *59*, 73–80. https://doi.org/10.1016/j.ceb.2019.03.009.
16. Jordan, K.L., Koss, D.J., Outeiro, T.F., and Giorgini, F. (2022). Therapeutic Targeting of Rab GTPases: Relevance for Alzheimer's Disease. Biomedicines *10*, 1141. https://doi.org/10.3390/biomedicines10051141.
17. Yoshimura, S.-i., Gerondopoulos, A., Linford, A., Rigden, D.J., and Barr, F. A. (2010). Family-wide characterization of the DENN domain Rab GDP-GTP exchange factors. J. Cell Biol. *191*, 367–381. https://doi.org/10.1083/jcb.201008051.
18. Kumar, R., Francis, V., Kulasekaran, G., Khan, M., Armstrong, G.A.B., and McPherson, P.S. (2022). A cell-based GEF assay reveals new substrates for DENN domains and a role for DENND2B in primary ciliogenesis. Sci. Adv. *8*, eabk3088. https://doi.org/10.1126/sciadv.abk3088.
19. Zhang, D., Iyer, L.M., He, F., and Aravind, L. (2012). Discovery of Novel DENN Proteins: Implications for the Evolution of Eukaryotic Intracellular Membrane Structures and Human Disease. Front. Genet. *3*, 283. https://doi.org/10.3389/fgene.2012.00283.
20. Gohring, I., Tagariello, A., Endele, S., Stolt, C.C., Ghassibe, M., Fisher, M., Thiel, C.T., Trautmann, U., Vikkula, M., Winterpacht, A., et al. (2010). Disruption of ST5 is associated with mental retardation and multiple congenital anomalies. J. Med. Genet. *47*, 91–98. https://doi.org/10.1136/jmg.2009.069799.
21. Anazi, S., Maddirevula, S., Salpietro, V., Asi, Y.T., Alsahli, S., Alhashem, A., Shamseldin, H.E., AlZahrani, F., Patel, N., Ibrahim, N., et al. (2017). Expanding the genetic heterogeneity of intellectual disability. Hum. Genet. *136*, 1419–1429. https://doi.org/10.1007/s00439-017-1843-2.
22. Romani, M., Mehawej, C., Mazza, T., Mégarbané, A., and Valente, E.M. (2016). Fork and bracket" syndrome expands the spectrum of SBF1-related sensory motor polyneuropathies. Neurol. Genet. *2*, e61. https://doi.org/10.1212/nxg.0000000000000061.
23. DeJesus-Hernandez, M., Mackenzie, I.R., Boeve, B.F., Boxer, A.L., Baker, M., Rutherford, N.J., Nicholson, A.M., Finch, N.A., Flynn, H., Adamson, J., et al. (2011). Expanded GGGGCC hexanucleotide repeat in noncoding region of C9ORF72 causes chromosome 9p-linked FTD and ALS. Neuron *72*, 245–256. https://doi.org/10.1016/j.neuron.2011.09.011.
24. Zhang, J., Zhang, K., Qi, L., Hu, Q., Shen, Z., Liu, B., Deng, J., Zhang, C., and Zhang, Y. (2019). DENN domain-containing protein FAM45A regulates the homeostasis of late/multivesicular endosomes. Biochim. Biophys. Acta Mol. Cell Res. *1866*, 916–929. https://doi.org/10.1016/j.bbamcr.2019.02.006.
25. Laulumaa, S., Kumpula, E.P., Huiskonen, J.T., and Varjosalo, M. (2024). Structure and interactions of the endogenous human Commander complex. Nat. Struct. Mol. Biol. *31*, 925–938. https://doi.org/10.1038/s41594-024-01246-1.
26. Boesch, D.J., Singla, A., Han, Y., Kramer, D.A., Liu, Q., Suzuki, K., Juneja, P., Zhao, X., Long, X., Medlyn, M.J., et al. (2024). Structural organization of the retriever-CCC endosomal recycling complex. Nat. Struct. Mol. Biol. *31*, 910–924. https://doi.org/10.1038/s41594-023-01184-4.
27. Healy, M.D., McNally, K.E., Butkovič, R., Chilton, M., Kato, K., Sacharz, J., McConville, C., Moody, E.R.R., Shaw, S., Planelles-Herrero, V.J., et al. (2023). Structure of the endosomal Commander complex linked to Ritscher-Schinzel syndrome. Cellule *186*, 2219–2237. https://doi.org/10.1016/j.cell.2023.04.003.
28. McDonald, F.J. (2021). Explosion in the complexity of membrane protein recycling. Am. J. Physiol., Cell. Physiol. *320*, C483–C494. https://doi.org/10.1152/ajpcell.00171.2020.
29. Chen, K.E., Healy, M.D., and Collins, B.M. (2019). Towards a molecular understanding of endosomal trafficking by Retromer and Retriever. Traffic *20*, 465–478. https://doi.org/10.1111/tra.12649.
30. McNally, K.E., and Cullen, P.J. (2018). Endosomal Retrieval of Cargo: Retromer Is Not Alone. Trends Cell Biol. *28*, 807–822. https://doi.org/10.1016/j.tcb.2018.06.005.
31. Mallam, A.L., and Marcotte, E.M. (2017). Systems-wide Studies Uncover Commander, a Multiprotein Complex Essential to Human Development. Cell Syst *4*, 483–494. https://doi.org/10.1016/j.cels.2017.04.006.
32. Singla, A., Fedoseienko, A., Giridharan, S.S.P., Overlee, B.L., Lopez, A., Jia, D., Song, J., Huff-Hardy, K., Weisman, L., Burstein, E., and Billadeau, D.D. (2019). Endosomal PI(3)P regulation by the COMMD/CCDC22/CCDC93 (CCC) complex controls membrane protein recycling. Nat. Commun. *10*, 4271. https://doi.org/10.1038/s41467-019-12221-6.
33. Ando, M., Funayama, M., Li, Y., Kashihara, K., Murakami, Y., Ishizu, N., Toyoda, C., Noguchi, K., Hashimoto, T., Nakano, N., et al. (2012). VPS35 mutation in Japanese patients with typical Parkinson's disease. Mov. Disord. *27*, 1413–1417. https://doi.org/10.1002/mds.25145.
34. Vilariño-Güell, C., Wider, C., Ross, O.A., Dachsel, J.C., Kachergus, J.M., Lincoln, S.J., Soto-Ortolaza, A.I., Cobb, S.A., Wilhoite, G.J., Bacon, J.A.,

et al. (2011). VPS35 Mutations in Parkinson Disease. Am. J. Hum. Genet. *89*, 162–167. https://doi.org/10.1016/j.ajhg.2011.06.001.

35. Zimprich, A., Benet-Pagès, A., Struhal, W., Graf, E., Eck, S.H., Offman, M. N., Haubenberger, D., Spielberger, S., Schulte, E.C., Lichtner, P., et al. (2011). A mutation in VPS35, encoding a subunit of the retromer complex, causes late-onset Parkinson disease. Am. J. Hum. Genet. *89*, 168–175. https://doi.org/10.1016/j.ajhg.2011.06.008.
36. McMillan, K.J., Gallon, M., Jellett, A.P., Clairfeuille, T., Tilley, F.C., McGough, I., Danson, C.M., Heesom, K.J., Wilkinson, K.A., Collins, B. M., and Cullen, P.J. (2016). Atypical parkinsonism–associated retromer mutant alters endosomal sorting of specific cargo proteins. J. Cell Biol. *214*, 389–399. https://doi.org/10.1083/jcb.201604057.
37. Voineagu, I., Huang, L., Winden, K., Lazaro, M., Haan, E., Nelson, J., McGaughran, J., Nguyen, L.S., Friend, K., Hackett, A., et al. (2012). CCDC22: a novel candidate gene for syndromic X-linked intellectual disability. Mol. Psychiatr. *17*, 4–7. https://doi.org/10.1038/mp.2011.95.
38. Kolanczyk, M., Krawitz, P., Hecht, J., Hupalowska, A., Miaczynska, M., Marschner, K., Schlack, C., Emmerich, D., Kobus, K., Kornak, U., et al. (2015). Missense variant in CCDC22 causes X-linked recessive intellectual disability with features of Ritscher-Schinzel/3C syndrome. Eur. J. Hum. Genet. *23*, 633–638. https://doi.org/10.1038/ejhg.2014.109.
39. Ropers, F., Derivery, E., Hu, H., Garshasbi, M., Karbasiyan, M., Herold, M., Nürnberg, G., Ullmann, R., Gautreau, A., Sperling, K., et al. (2011). Identification of a novel candidate gene for non-syndromic autosomal recessive intellectual disability: the WASH complex member SWIP. Hum. Mol. Genet. *20*, 2585–2590. https://doi.org/10.1093/hmg/ddr158.
40. Elliott, A.M., Simard, L.R., Coghlan, G., Chudley, A.E., Chodirker, B.N., Greenberg, C.R., Burch, T., Ly, V., Hatch, G.M., and Zelinski, T. (2013). A novel mutation in KIAA0196: identification of a gene involved in Ritscher-Schinzel/3C syndrome in a First Nations cohort. J. Med. Genet. *50*, 819–822. https://doi.org/10.1136/jmedgenet-2013-101715.
41. Kato, K., Oka, Y., Muramatsu, H., Vasilev, F.F., Otomo, T., Oishi, H., Kawano, Y., Kidokoro, H., Nakazawa, Y., Ogi, T., et al. (2020). Biallelic VPS35L pathogenic variants cause 3C/Ritscher-Schinzel-like syndrome through dysfunction of retriever complex. J. Med. Genet. *57*, 245–253. https://doi.org/10.1136/jmedgenet-2019-106213.
42. Williams, E.T., Chen, X., Otero, P.A., and Moore, D.J. (2022). Understanding the contributions of VPS35 and the retromer in neurodegenerative disease. Neurobiol. Dis. *170*, 105768. https://doi.org/10.1016/j.nbd.2022.105768.
43. Qi, Y., Wang, J.K., McMillian, M., and Chikaraishi, D.M. (1997). Characterization of a CNS cell line, CAD, in which morphological differentiation is initiated by serum deprivation. J. Neurosci. *17*, 1217–1225.
44. Wang, H., and Oxford, G.S. (2000). Voltage-dependent ion channels in CAD cells: A catecholaminergic neuronal line that exhibits inducible differentiation. J. Neurophysiol. *84*, 2888–2895. https://doi.org/10.1152/jn.2000.84.6.2888.
45. Mews, P., Donahue, G., Drake, A.M., Luczak, V., Abel, T., and Berger, S.L. (2017). Acetyl-CoA synthetase regulates histone acetylation and hippocampal memory. Nature *546*, 381–386. https://doi.org/10.1038/nature22405.
46. Chesta, M.E., Carbajal, A., Arce, C.A., and Bisig, C.G. (2014). Serum-induced neurite retraction in CAD cells–involvement of an ATP-actin retractile system and the lack of microtubule-associated proteins. FEBS J. *281*, 4767–4778. https://doi.org/10.1111/febs.12967.
47. Soppina, V., Norris, S.R., Dizaji, A.S., Kortus, M., Veatch, S., Peckham, M., and Verhey, K.J. (2014). Dimerization of mammalian kinesin-3 motors results in superprocessive motion. Proc. Natl. Acad. Sci. USA *111*, 5562–5567. https://doi.org/10.1073/pnas.1400759111.
48. Blasius, T.L., Yue, Y., and Verhey, K. (2019). Microtubule binding of the kinesin-4 KIF7 and its regulation by autoinhibition. Preprint at bioRxiv. https://doi.org/10.1101/772327.
49. Muresan, Z., and Muresan, V. (2006). Neuritic deposits of amyloid-beta peptide in a subpopulation of central nervous system-derived neuronal cells. Mol. Cell Biol. *26*, 4982–4997. https://doi.org/10.1128/mcb.00371-06.
50. Tuladhar, R., Yeu, Y., Tyler Piazza, J., Tan, Z., Rene Clemenceau, J., Wu, X., Barrett, Q., Herbert, J., Mathews, D.H., Kim, J., et al. (2019). CRISPR-Cas9-based mutagenesis frequently provokes on-target mRNA misregulation. Nat. Commun. *10*, 4056. https://doi.org/10.1038/s41467-019-12028-5.
51. Latremoliere, A., Cheng, L., DeLisle, M., Wu, C., Chew, S., Hutchinson, E. B., Sheridan, A., Alexandre, C., Latremoliere, F., Sheu, S.H., et al. (2018). Neuronal-Specific TUBB3 Is Not Required for Normal Neuronal Function but Is Essential for Timely Axon Regeneration. Cell Rep. *24*, 1865–1879. https://doi.org/10.1016/j.celrep.2018.07.029.
52. Zhang, L., and Elias, J.E. (2017). Relative Protein Quantification Using Tandem Mass Tag Mass Spectrometry. Methods Mol. Biol. *1550*, 185–198. https://doi.org/10.1007/978-1-4939-6747-6_14.
53. Szklarczyk, D., Gable, A.L., Nastou, K.C., Lyon, D., Kirsch, R., Pyysalo, S., Doncheva, N.T., Legeay, M., Fang, T., Bork, P., et al. (2021). The STRING database in 2021: customizable protein-protein networks, and functional characterization of user-uploaded gene/measurement sets. Nucleic Acids Res. *49*, D605-d612. https://doi.org/10.1093/nar/gkaa1074.
54. Ohnuma, S.i., and Harris, W.A. (2003). Neurogenesis and the cell cycle. Neuron *40*, 199–208. https://doi.org/10.1016/s0896-6273(03)00632-9.
55. Gupton, S.L., and Gertler, F.B. (2010). Integrin signaling switches the cytoskeletal and exocytic machinery that drives neuritogenesis. Dev. Cell *18*, 725–736. https://doi.org/10.1016/j.devcel.2010.02.017.
56. Courtland, J.L., Bradshaw, T.W., Waitt, G., Soderblom, E.J., Ho, T., Rajab, A., Vancini, R., Kim, I.H., and Soderling, S.H. (2021). Genetic disruption of WASHC4 drives endo-lysosomal dysfunction and cognitive-movement impairments in mice and humans. Elife *10*, e61590. https://doi.org/10.7554/eLife.61590.
57. Ajoolabady, A., Lindholm, D., Ren, J., and Pratico, D. (2022). ER stress and UPR in Alzheimer's disease: mechanisms, pathogenesis, treatments. Cell Death Dis. *13*, 706. https://doi.org/10.1038/s41419-022-05153-5.
58. Costa, C.A.D., Manaa, W.E., Duplan, E., and Checler, F. (2020). The Endoplasmic Reticulum Stress/Unfolded Protein Response and Their Contributions to Parkinson's Disease Physiopathology. Cell *9*, 2495. https://doi.org/10.3390/cells9112495.
59. Pfenninger, K.H., and Johnson, M.P. (1983). Membrane biogenesis in the sprouting neuron. I. Selective transfer of newly synthesized phospholipid into the growing neurite. J. Cell Biol. *97*, 1038–1042. https://doi.org/10.1083/jcb.97.4.1038.
60. Kim, G., Choe, Y., Park, J., Cho, S., and Kim, K. (2002). Activation of protein kinase A induces neuronal differentiation of HiB5 hippocampal progenitor cells. Brain research. Brain Res. Mol. Brain Res. *109*, 134–145. https://doi.org/10.1016/s0169-328x(02)00550-8.
61. Ahn, J.Y. (2014). Neuroprotection signaling of nuclear akt in neuronal cells. Exp. Neurobiol. *23*, 200–206. https://doi.org/10.5607/en.2014.23.3.200.
62. Jin, L., Han, S., Lv, X., Li, X., Zhang, Z., Kuang, H., Chen, Z., Lv, C.A., Peng, W., Yang, Z., et al. (2023). The muscle-enriched myokine Musclin impairs beige fat thermogenesis and systemic energy homeostasis via Tfr1/PKA signaling in male mice. Nat. Commun. *14*, 4257. https://doi.org/10.1038/s41467-023-39710-z.
63. Dominguez, N., van Weering, J.R.T., Borges, R., Toonen, R.F.G., and Verhage, M. (2018). Dense-core vesicle biogenesis and exocytosis in neurons lacking chromogranins A and B. J. Neurochem. *144*, 241–254. https://doi.org/10.1111/jnc.14263.
64. Longhena, F., Faustini, G., Brembati, V., Pizzi, M., Benfenati, F., and Bellucci, A. (2021). An updated reappraisal of synapsins: structure, function and role in neurological and psychiatric disorders. Neurosci. Biobehav. Rev. *130*, 33–60. https://doi.org/10.1016/j.neubiorev.2021.08.011.

65. Arimura, N., Kimura, T., Nakamuta, S., Taya, S., Funahashi, Y., Hattori, A., Shimada, A., Ménager, C., Kawabata, S., Fujii, K., et al. (2009). Anterograde transport of TrkB in axons is mediated by direct interaction with Slp1 and Rab27. Dev. Cell *16*, 675–686. https://doi.org/10.1016/j.devcel.2009.03.005.

66. Yu, E., Kanno, E., Choi, S., Sugimori, M., Moreira, J.E., Llinás, R.R., and Fukuda, M. (2008). Role of Rab27 in synaptic transmission at the squid giant synapse. Proc. Natl. Acad. Sci. USA *105*, 16003–16008. https://doi.org/10.1073/pnas.0804825105.

67. Magtanong, L., Ho, C.H., Barker, S.L., Jiao, W., Baryshnikova, A., Bahr, S., Smith, A.M., Heisler, L.E., Choy, J.S., Kuzmin, E., et al. (2011). Dosage suppression genetic interaction networks enhance functional wiring diagrams of the cell. Nat. Biotechnol. *29*, 505–511. https://doi.org/10.1038/nbt.1855.

68. Roy, D., and Tedeschi, A. (2021). The Role of Lipids, Lipid Metabolism and Ectopic Lipid Accumulation in Axon Growth, Regeneration and Repair after CNS Injury and Disease. Cells *10*, 1078. https://doi.org/10.3390/cells10051078.

69. Meltzer, S., Bagley, J.A., Perez, G.L., O'Brien, C.E., DeVault, L., Guo, Y., Jan, L.Y., and Jan, Y.N. (2017). Phospholipid Homeostasis Regulates Dendrite Morphogenesis in Drosophila Sensory Neurons. Cell Rep. *21*, 859–866. https://doi.org/10.1016/j.celrep.2017.09.089.

70. Palomo-Guerrero, M., Fadó, R., Casas, M., Pérez-Montero, M., Baena, M., Helmer, P.O., Domínguez, J.L., Roig, A., Serra, D., Hayen, H., et al. (2019). Sensing of nutrients by CPT1C regulates late endosome/lysosome anterograde transport and axon growth. Elife *8*, e51063. https://doi.org/10.7554/eLife.51063.

71. Pinson, A., Xing, L., Namba, T., Kalebic, N., Peters, J., Oegema, C.E., Traikov, S., Reppe, K., Riesenberg, S., Maricic, T., et al. (2022). Human TKTL1 implies greater neurogenesis in frontal neocortex of modern humans than Neanderthals. Science *377*, eabl6422. https://doi.org/10.1126/science.abl6422.

72. Sekine, Y., Lin-Moore, A., Chenette, D.M., Wang, X., Jiang, Z., Cafferty, W. B., Hammarlund, M., and Strittmatter, S.M. (2018). Functional Genome-wide Screen Identifies Pathways Restricting Central Nervous System Axonal Regeneration. Cell Rep. *23*, 415–428. https://doi.org/10.1016/j.celrep.2018.03.058.

73. Rojas, R., van Vlijmen, T., Mardones, G.A., Prabhu, Y., Rojas, A.L., Mohammed, S., Heck, A.J.R., Raposo, G., van der Sluijs, P., and Bonifacino, J.S. (2008). Regulation of retromer recruitment to endosomes by sequential action of Rab5 and Rab7. J. Cell Biol. *183*, 513–526. https://doi.org/10.1083/jcb.200804048.

74. Schneider, C.A., Rasband, W.S., and Eliceiri, K.W. (2012). NIH Image to ImageJ: 25 years of image analysis. Nat. Methods *9*, 671–675. https://doi.org/10.1038/nmeth.2089.

75. Meijering, E., Jacob, M., Sarria, J.C.F., Steiner, P., Hirling, H., and Unser, M. (2004). Design and validation of a tool for neurite tracing and analysis in fluorescence microscopy images. Cytometry A. *58*, 167–176. https://doi.org/10.1002/cyto.a.20022.

76. Labun, K., Montague, T.G., Krause, M., Torres Cleuren, Y.N., Tjeldnes, H., and Valen, E. (2019). CHOPCHOP v3: expanding the CRISPR web toolbox beyond genome editing. Nucleic Acids Res. *47*, W171-w174. https://doi.org/10.1093/nar/gkz365.

77. Sun, S., Li, Q., Liu, G., Huang, X., Li, A., Guo, H., Qi, L., Zhang, J., Song, J., Su, X., and Zhang, Y. (2024). Endosomal protein DENND10/FAM45A integrates extracellular vesicle release with cancer cell migration. BMC Biol. *22*, 154. https://doi.org/10.1186/s12915-024-01948-4.

78. Ran, F.A., Hsu, P.D., Wright, J., Agarwala, V., Scott, D.A., and Zhang, F. (2013). Genome engineering using the CRISPR-Cas9 system. Nat. Protoc. *8*, 2281–2308. https://doi.org/10.1038/nprot.2013.143.

79. Sanjana, N.E., Shalem, O., and Zhang, F. (2014). Improved vectors and genome-wide libraries for CRISPR screening. Nat. Methods *11*, 783–784. https://doi.org/10.1038/nmeth.3047.

80. Kuleshov, M.V., Jones, M.R., Rouillard, A.D., Fernandez, N.F., Duan, Q., Wang, Z., Koplev, S., Jenkins, S.L., Jagodnik, K.M., Lachmann, A., et al. (2016). Enrichr: a comprehensive gene set enrichment analysis web server 2016 update. Nucleic Acids Res. *44*, W90–W97. https://doi.org/10.1093/nar/gkw377.

81. Shannon, P., Markiel, A., Ozier, O., Baliga, N.S., Wang, J.T., Ramage, D., Amin, N., Schwikowski, B., and Ideker, T. (2003). Cytoscape: a software environment for integrated models of biomolecular interaction networks. Genome Res. *13*, 2498–2504. https://doi.org/10.1101/gr.1239303.

STAR★METHODS

KEY RESOURCES TABLE

REAGENT or RESOURCE	SOURCE	IDENTIFIER
Antibodies		
TUBB3	Beyotime	Cat # AT809; Clone Tuj1; RRID:AB_2893434
Rab27a	Proteintech	Cat # 17817-1-AP; RRID:AB_2176728
Rab27b	Proteintech	Cat # 13412-1-AP; RRID:AB_2176732
CD63	BD Biosciences	Cat # 556019; RRID:AB_396297
Map2	Cell Signaling Technology	Cat # 8707T; Clone D5G1; RRID:AB_2722660
Tau	EMD Millipore	Cat # MAB3420; Clone PC1C6; RRID:AB_10947848
Alexa Fluor 555 donkey anti-mouse IgG	Beyotime	Cat# A0460; RRID:AB_2890133
Alexa Fluor 555 donkey anti-rabbit IgG	Beyotime	Cat# A0453; RRID:AB_2890132
Alexa Fluor 488 goat anti-rabbit IgG	Beyotime	Cat# A0423; RRID:AB_2891323
Alexa Fluor 647 goat anti-mouse IgG	Beyotime	Cat# A0473; RRID:AB_2891322
phospho-PKA Substrates	Cell Signaling Technology	Cat# 9624; RRID:AB_331817
Akt	Ruiying	Cat# RLT0178; RRID:AB_2814756
phosphor-Akt (Ser473)	Ruiying	Cat# RLP0006; RRID:AB_2814755
CHGB	Proteintech	Cat# 14968-1-AP; RRID:AB_2081138
SYN-1	Ruiying	RLT4483; RRID:AB_3683540
TH	Proteintech	Cat# 25859-1-AP; RRID:AB_2716568
GAPDH	Ruiying	RLM3029; RRID: AB_3683541
actin	Ruiying	RLT0099; RRID:AB_2885029
FLAG	Beyotime	AF0036; RRID: AB_3683542
GFP/Citrine	Proteintech	Cat# 50430-2-AP; RRID:AB_11042881
Chemicals, peptides, and recombinant proteins		
DMEM/F12	Invitrogen	Cat# C11330500BT
fetal bovine Serum	Sijiqing	Cat# BC-002
Penicillin/Streptomycin/L-Glutamine	HyClone	Cat# SV30082.01
0.25% Trypsin-EDTA	Gibco	Cat# 25200056
GlutaMAX	Gibco	Cat# 35050061
penicillin–streptomycin	Gibco	Cat# 15140122
poly-D-lysine	Sigma	Cat# P6407
Neurobasal medium	Gibco	Cat# 21103049
B27	Gibco	Cat# 17504044
PEI Max	Polysciences Inc	Cat# 24765
Lipofectamine 2000	Invitrogen	Cat# 11668030
TRITC Phalloidin	Solarbio	Cat# CA1610
Deposited data		
Raw mass spectrometry proteomics data	This paper	ProteomeXchange Consortium: PXD038623
Experimental models: Cell lines		
Mouse: CAD cells	Laboratory of Dr. Kristen Verhey	ECACC: 08100805; RRID:CVCL_0199
Human: HeLa cells	Laboratory of Dr. Lois Weisman	ATCC: CCL-2; RRID:CVCL_0030
Human: HEK293T cells	Laboratory of Dr. Lois Weisman	ATCC: CRL-3216; RRID:CVCL_0063
Experimental models: Organisms/strains		
C57BL/6J	SLAC Laboratory Animal Company (Shanghai, China)	RRID:IMSR_JAX:000664

(*Continued on next page*)

Continued

REAGENT or RESOURCE	SOURCE	IDENTIFIER
Oligonucleotides		
Primers for quantitative PCR and cloning. See Table S5	This paper	N/A
Recombinant DNA		
pGPU6/GFP/*Neo*	GenePharma	Cat #C01001
TOPO Blunt vector	Aidlab	CV17
Software and algorithms		
ImageJ 1.53n	Schneider et al.[74]	https://imagej.nih.gov/ij/
NeuroJ v1.4.3	Meijering et al.[75]	https://imagescience.org/meijering/software/neuronj/
R v4.0.3	R Consortium	https://www.r-project.org/
Cytoscape v3.8.0	Cytoscape Consortium	https://cytoscape.org/download.html
GraphPad Prism 9	GraphPad	https://www.graphpad.com/

EXPERIMENTAL MODEL AND STUDY PARTICIPANT DETAILS

Cell culture

Mouse CAD cells[43] (RRID: CVCL_0199) were cultured in DMEM/F12 medium (Invitrogen, Cat. No. C11330500BT, Waltham, Massachusetts, USA) supplemented with 10% fetal bovine Serum (FBS, Sijiqing, BC-002, Hangzhou, China) and 1x Penicillin/Streptomycin/L-Glutamine (HyClone, SV30082.01, Logan, Utah, USA) at 37°C in a 5% carbon dioxide incubator. Neuronal differentiation of CAD cells was initiated by serum deprivation. Human HeLa (ATCC No. CCL-2) and HEK293T (ATCC No. CRL-3216) cells were cultured in DMEM medium (Invitrogen, C11965500BT) supplemented as above.

Primary cortical neurons

All animal protocols were approved by the Animal Care and Use Committee at Soochow University (202410A0190). Pregnant C57BL/6J female mice were purchased from SLAC Laboratory Animal Company (Shanghai, China). Brains from E18 embryos were isolated aseptically and meninges were removed. Cortices were dissected out by forceps and digested with 0.25% Trypsin-EDTA (Gibco, 25200056) for 12 min with occasional inversion. The trypsin solution was removed by pipetting and resuspended in DMEM/F12 medium with 10% FBS, 1% GlutaMAX (Gibco, 35050061), and 1% penicillin–streptomycin (Gibco, 15140122) to end the digestion. The cell suspension was filtered through a sterile 40 μm cell strainer (Biosharp, BS-40-XBS) and plated on six-well tissue culture dishes precoated with 20 ng/mL poly-D-lysine (Sigma, P6407) at 1.5×10^6 cells per well. After 4 h, the medium was replaced with Neurobasal medium (Gibco, 21103049) supplemented with 2% B27 (Gibco, 17504044), 1% GlutaMAX, and 1% penicillin–streptomycin in a 5% CO_2 incubator at 37°C.

METHOD DETAILS

Plasmids

The following plasmids, 3xFLAG-DENND10, mCherry-DENND10, Cit-Rab27a-Q78L, Cit-Rab27b-Q78L, Cit-Rab27a-T23N, Cit-Rab27b-T23N were described in a previous study.[24] The human *CCDC22* gene was amplified from cDNA using the following primers: 5′-CCG CAA GCT TCG ATG GAG GAG GCG GAC CG-3′ and 5′- CCG CGG ATC CTC AGG CCT CCC GGA CCC-3′ and cloned into HindIII/BamHI digested pCitrine-C1. The shRNA knockdown pGPU6/GFP/*Neo* plasmids were purchased from GenePharma (Suzhou, China), which co-express the GFP protein to allow simultaneous assessment of neuron morphology after transfection. The following shRNA targeting sequences were used: mouse *Dennd10* sh1: GCA ACAGA CCA GAC CTC TAT G; mouse *Dennd10* sh2: GCG ATT TCC ACC CGC AAC AGA; mouse *Ccdc22* sh1: GGA AAC CGA GTG CCG ACA AAG; mouse *Ccdc22* sh2: GCT GCC CTG CAT GAG AAT TGC; non-targeting control sequence: GTT CTC CGA ACG TGT CAC GT.

Transfection in cell lines

Transfection experiments in CAD, HeLa, and HEK293T cells were performed with PEI Max (Polysciences Inc., 24765, Warrington, PA, USA). Briefly, transfection mixes were prepared according to the manufacturer's instruction at the ratio of 1:4 (μg DNA: μl PEI Max) in Opti-MEM medium and added to cells in the absence of serum and antibiotics. After 4 h, cells were returned to normal medium for 24-48 h to allow the expression of proteins of interest. For imaging Cit-CCDC22 and mCherry-DENND10, cells were briefly treated with 0.1% saponin for 1 min to decrease cytosolic signals before fixation.

Transfection in primary neurons

Primary cortical neurons were transfected with Lipofectamine 2000 (Invitrogen, 11668030) according to the manufacturer's instruction at 2.5 μg DNA and 8 μL Lipofectamine per well in a six-well format on the 2nd day after initial plating. The transfection mix was replaced with normal medium after 2 h. Neurons were replated at 24 h post-transfection by gentle digestion with 0.125% Trypsin-EDTA solution for 30 s and re-seeded onto coverslips coated with poly-D-lysine. Neurons were then cultured for two days before fixation and immunofluorescence experiments.

CRIPSR-mediated gene editing

Two sgRNAs targeting the first exon of mouse *Dennd10* gene were designed using the web tool CHOPCHOP[76]: 5′-AAG TCC CGT CCC TTC CGG CA-3′ and 5′-CGG AGT CGG GCT GAT CGG TG-3'. The same sequences have been used to knockout mouse *Dennd10* genes successfully in a previous study.[77] A short DNA fragment containing the guide RNA scaffold sequence[78] and U6 promoter (Table S5) was synthesized at Synbio Technologies (Suzhou, China). After PCR amplification that added the two sgRNA sequences (Table S5) at the ends, the fragment was cloned into LentiCRISPR v2 vector[79] digested with BsmBI. Lentiviral particles were produced in HEK293T cells by co-transfection of the recombinant LentiCRISPR v2 plasmid with two packaging plasmids, pMD2.G and psPAX2, at 4:2:3. The pMD2.G plasmid expresses VSV-G envelop proteins for pseudotyping, while psPAX2 expresses Gag, Pol, Rev, and Tat proteins for packaging. Viral-like particles were collected at 36 to 72 h and used to transduce CAD cells. After 24 h, CAD cells were selected with 2 μg/mL puromycin for 5–7 days. Clonal cell lines were obtained with serial dilution and screened by qPCR for low *Dennd10* gene expression. To examine the gene editing sites, genomic DNA was extracted, PCR amplified with the following primers: 5′-AGC GTA GAA AGG CTG CAA GA-3′and 5′-CCC AAG TCT AGC CTC TCC CT-3′, cloned into the TOPO Blunt vector (Aidlab, CV17, Beijing, China) and sequenced.

Neurite outgrowth

CAD cells were plated in six-well plates at 3×10^5 cells per well. To enhance neurite visualization, cells at 50–60% confluency were transfected with Citrine or Citrine-tagged vector using PEI Max. For each well, 1 μg DNA and 4 μL PEI Max were mixed in 500 μL of Opti-MEM medium and applied for 4 h in the absence of serum and antibiotics. Afterward, the medium was replaced with standard growth medium. When transfected CAD cells reached 80% confluency, they were differentiated by switching to medium without FBS for 36–48 h. Cells were washed with PBS, fixed with 3.7% PFA for 15 min, and imaged on a Leica SP8 confocal microscope. Around 6–12 random fields were taken for each experiment. To quantify neurite outgrowth, the longest neurite of each cell was traced with ImageJ.[74] The number of neurites per cell was counted manually.

For primary neurons, dendrites and axons were labeled with rabbit anti-Map2 and mouse anti-Tau antibodies, respectively. Dendrite length and number were measured with the NeuroJ plugin v1.4.3[75] of ImageJ.

TMT based proteomics

NC and sgDennd10_No2 CAD cells were grown to 80% confluency in the undifferentiated state, or differentiated for 48 h as indicated above. These undifferentiated and differentiated CAD cells were washed with PBS, scraped off the plates, and flash-frozen in liquid N_2. Samples were lysed in 8 M urea and 1% protease inhibitors by sonication, and centrifuged at 12,000 g for 10 min at 4°C to remove cell debris. Protein concentration was determined with the BCA kit. Equal masses of proteins from each sample were precipitated with cold acetone at −20°C. After drying, the pellet was resuspended in 200 mM TEAB, reduced in 5 mM DTT for 30 min at 56°C, followed by alkylation with 11 mM IAA for 15 min in the dark. Proteins were digested with trypsin at a ratio of 1:50 (m/m) overnight. The resultant peptides were desalted with a Strata X C18 column, vacuum dried, resuspended in 0.5M TEAB, and labeled with the TMT-16plex kit according to the manufacturer's instructions. Labeled peptides were fractionated with reverse-phase HPLC (Agilent 300Extend-C18) on a gradient of 8%–32% acetonitrile (pH 9). Fractions were further separated with EASY-nLC 1200 ultra-high performance liquid phase system (mobile phase A: 0.1% formic acid, 2% acetonitrile; mobile phase B: 0.1% formic acid, 90% acetonitrile). The following gradient was used at a flow rate of 500.00 nL/min: 0–4 min, 7%–11% B; 4–53 min, 11%–32% B; 53–57 min, 32%–80% B; 57–60 min, 80% B. The peptides were ionized by an NSI ion source at 2.3 kV and analyzed with the Orbitrap Exploris 480 mass spectrometer. The scan range was set at 400–1200 m/z with a resolution of 60, 000.00. MS/MS scan was performed with a DDA workflow (starting at 100 m/z, resolution at 45, 000.00). The following parameters were used: automatic gain control at 100; intensity threshold at 5E4 ions/s; maximum injection time at 50 ms; dynamic exclusion time at 30s. MS/MS data was searched using PD 2.4 against the Mus_musculus_10090 database (17045 sequences). The following settings were used: enzyme digestion, Trypsin (Full); number of missed cleavage sites, 2; minimum length, 7 amino acid residues; maximum number of modification, 5; mass tolerance for precursor ions, 10.0 ppm for first search and 5 ppm for main search; mass tolerance of fragment ions, 0.02 Da; quantitative method, TMT-16plex; FDR of both protein identification and PSM identification; 1%. The mass spectrometry analysis was performed by the PTM Biolab Inc (Hangzhou, China).

Bioinformatics data analysis of proteomics

The analysis of the proteomic dataset was performed in R (Version 4.0.3). To identify differentially expressed proteins (DEPs), two-way ANOVA was performed using the "lm" function in base R for every quantifiable protein with the following formula: "∼ Genotype + Differentiation + Genotype: Differentiation". Raw *p* values were adjusted for multi-comparison with the false discovery rate (FDR)

method using the "p.adjust" function. Scatterplots, bar plots, and volcano plots were made with the ggplot2 package. To visualize the over-crowded region in the scatterplots, 2D histograms were drawn using the "stat_bin2d" function in ggplot2. PCA was calculated with the "prcomp" function in base R. Heatmaps were drawn using the pheatmap package. Pathway enrichment was carried out on lists of DEPs using the enrichR package,[80] in which the "GO_Biological_Process_2021" library was specified as the ontology database to search. Lists of DEPs were also used as the input for the STRING database[53] to visualize interactions/associations among these proteins. The resultant interaction network was then imported into the Cytoscape 3.8.0 software,[81] in which protein nodes were colored by their respective fold changes.

Immunoprecipitation

To screen for DENND10 interacting proteins, HEK293T cells were transfected with 3xFLAG-DENND10/FAM45A[24] or empty pcDNA3.1 vector for 24 h. Proteins were extracted by triturating with a syringe needle (1.4 by 13 mm) about 20 times in the lysis buffer (10 mM HEPES at pH 8.0, 100 mM NaCl, 1 mM EDTA, and 1X protease inhibitor cocktail). Cell lysates were spun down at 20, 000 g for 20 min at 4°C. Protein concentrations of the supernatant were measured by BCA assay and adjusted to the same level. Equal amounts of the supernatant were incubated with anti-FLAG M2 affinity gel (Sigma A2220) overnight at 4°C on a rotator. The gel beads were spun down at 2, 000 g for 3 min at 4°C and washed with the washing buffer (50% HEPES lysis buffer, 50% PBS, and 0.1% Triton X-100) for three times. Proteins were eluted from the beads by heating in non-reducing Laemmli buffer at 95°C for 5 min.

To identify proteins that co-precipitated with DENND10, samples were run into the separating gel of SDS-PAGE for 1.5 cm and then gel slices were cut out for mass spectrometry analysis by PTM Biolab Inc (Hangzhou, China). Gel pieces were dehydrated with 100% acetonitrile, reduced with 10 mM dithiothreitol, alkylated with 55 mM iodoacetamide, and digested with trypsin at 37°C overnight. Peptides were separated by a home-made reversed-phase analytical column on an EASY-nLC 1000 UPLC system, ionized at 2.0 kV, and analyzed with the Q Exactive Plus (Thermo Scientific) mass spectrometer. The following parameters were used: m/z scan range at 350 to 1800; precursor resolution at 70, 000; fragment peptide resolution at 17, 500, and automatic gain control at 5E4. The resulting MS/MS spectra were searched against SwissProt *Homo sapiens* database (20422 sequences) with Proteome Discoverer 1.3.

For assessing the interaction between DENND10 and CCDC22, 3xFLAG-DENND10 was co-transfected with Citrine-CCDC22 or pCitrine-C1 vector into HEK293T cells, immunoprecipitated as above and immunoblotted with rabbit anti-FLAG (Beyotime, AF0036) and anti-GFP/Citrine (Proteintech, 50430-2-AP).

Immunofluorescence

CAD cells were seeded on coverslips situated in six-well plates at 3×10^5 cells per well, grown until ~80% confluency, and differentiated as above for 36–48 h. Differentiated cells were washed with PBS, and fixed with 3.7% PFA for 15 min at room temperature. Permeabilization was performed by incubation in 0.1% Triton X-100 for 5 min to allow antibody entry into cells. Nonspecific binding was blocked by 2% normal goat serum (Solarbio, SL038, Beijing, China) or normal donkey serum (Solarbio, SL4) for 1 h. Coverslips were then incubated with primary antibodies diluted at 1:200 in the blocking solution at 4°C overnight, followed by incubation with fluorescent secondary antibodies (1:400) at room temperature for 1 h, and then incubation with 0.1 μg/mL DAPI/PBS for 5 min to stain the nuclei. Finally, coverslips were mounted with SlowFade Diamond Antifade Mountant with DAPI (Invitrogen, S36968) and imaged on a Leica SP8 confocal microscope. The following primary antibodies were used: TUBB3 (Beyotime, AT809, Clone Tuj1, Shanghai, China), Rab27a (Proteintech, 17817-1-AP), Rab27b (Proteintech, 13412-1-AP), CD63 (BD Biosciences, 556019), Map2 (Cell Signaling Technology, Clone D5G1, 8707T, Danvers, MA, USA), Tau (EMD Millipore, Clone PC1C6, MAB3420). The following secondary antibodies were used: Alexa Fluor 555 donkey anti-mouse IgG (Beyotime, A0460), Alexa Fluor 555 donkey anti-rabbit IgG (Beyotime, A0453), Alexa Fluor 488 goat anti-rabbit IgG (Beyotime, A0423), and Alexa Fluor 647 goat anti-mouse IgG (Beyotime, A0473).

In order to quantify neurite tip localization of Rab27a and Rab27b, cells were stained in 100nM TRITC Phalloidin (Solarbio, CA1610) for 30min in the dark before mounting for visualizing cell outlines. Six to eight random fields were imaged per coverslip with a 63× objective (N.A. = 1.4). Neurons were categorized into two classes: tip and non-tip localization of Rab27a or Rab27b. The percentage of neurons with Rab27a/Rab27b localization at neurite tips was calculated for each independent experiment.

qRT-PCR

Quantitative reverse transcription PCR (qRT-PCR) was used to measure the expression of *Dennd10* and *Ccdc22* genes. Total RNA was prepared with Total RNA Extractor (Sangon, SK1312, Shanghai, China) from non-differentiated and differentiated CAD cells. One microgram RNA was reverse-transcribed with Primescript RT master mix (Takara, RR036A, Otsu, Japan). The resulting cDNA was amplified with TB Green Premix Ex Taq II (Takara, RR820A, Japan) in an ABI 7500 Real-Time PCR System (Applied Biosystems, Bedford, MA, USA). The *Rpl32* gene was used as the internal control. The following primers were used: *Dennd10*-F: GTT GTG GCA ATG GAC ACC CA; *Dennd10*-R: GGC TGT CGT GGA AGG ATA ACA; *Ccdc22*-F: GAC TCT GCG AGC TTT CAC CA; *Ccdc22*-R: GCT CAC TGG GAT AGA GGA AGT; *Rpl32*-F: TTA AGC GAA ACT GGC GGA AAC; *Rpl32*-R: TTG TTG CTC CCA TAA CCG ATG. The $2^{-\Delta\Delta Ct}$ method was used to calculate relative gene expression.

Western blotting

Cells were scraped into the lysis buffer (50 mM Tris pH 7.5, 150 mM NaCl, 0.5% Triton X-100, 1 mM PMSF, 10 mM NaF, 1 mM Na_3VO_4, and 1x proteinase inhibitor cocktail), rocked for 1 h at 4°C and cleared by centrifugation at 14, 000 rpm for 10 min. Proteins

were separated on SDS-PAGE and transferred to PVDF membranes. Blocking was performed by incubation with 5% non-fat milk/0.1% Tween 20/TBS. The following primary antibodies were used at 1: 2000 for immunoblotting: phospho-PKA Substrates (Cell Signaling Technology, Clone 100G7E, #9624), total Akt (Ruiying, RLT0178, Suzhou, China), phosphor-Akt (Ser473) (Ruiying, RLP0006), TUBB3 (Beyotime, AT809), CHGB (Proteintech, 14968-1-AP), SYN-1 (Ruiying, RLT4483), TH (Proteintech, 25859-1-AP), GAPDH (Ruiying, RLM3029), and actin (Ruiying, RLT0099). After incubation with corresponding HRP-conjugated secondary antibodies, the blot was developed with the Immobilon Western Chemiluminescent HRP Substrate (Merck, WBKLS0050, Darmstadt, Germany).

QUANTIFICATION AND STATISTICAL ANALYSIS

Statistics

Statistical analysis and data plotting were carried out in GraphPad Prism 9. Data are presented as mean ± SD. Statistical tests and exact values of n-numbers are described in the figure legends. Statistical Significance for comparisons among more than three groups was determined using ANOVA followed by post hoc multiple-comparison tests. Neurite lengths and numbers were displayed with violin plots to show individual points. A value of $p < 0.05$ was considered statistically significant.